CHALMERS
UNIVERSITY OF TECHNOLOGY

Effects of Heat Treatment on Residual Stresses in Additive Manufacturing

Master's thesis in Materials Engineering

Rasmus Kristensen

DEPARTMENT OF INDUSTRIAL AND MATERIALS SCIENCE

CHALMERS UNIVERSITY OF TECHNOLOGY
Gothenburg, Sweden 2024
www.chalmers.se

Master's thesis 2024

Effects of Heat Treatment on Residual Stresses in Additive Manufacturing

RASMUS KRISTENSEN

CHALMERS
UNIVERSITY OF TECHNOLOGY

Department of Industrial and Materials Science
Division of Materials- and Manufacturing Technology
Chalmers University of Technology
Gothenburg, Sweden 2024

Effects of Heat Treatment on Residual
Stresses in Additive Manufacturing
RASMUS KRISTENSEN

Supervisors: Henrik Karlsson, Volvo Group Trucks Technology
Rasha Alkaisee, Volvo Group Trucks Technology
Examiner: Eduard Hryha, Industrial and Materials Science, Chalmers University of Technology

Master's Thesis 2024
Department of Industrial and Materials Science
Division of Materials- and Manufacturing Technology
Chalmers University of Technology
SE-412 96 Gothenburg
Telephone +46 31 772 1000

Cover: Yoke for diesel injector, printed with PBF-LB in 42CrMo4.

Typeset in LaTeX
Printed by Chalmers Reproservice
Gothenburg, Sweden 2024

Effects of Heat Treatment on Residual Stresses in Additive Manufacturing
RASMUS KRISTENSEN
Department of Industrial and Material Science
Chalmers University of Technology

Abstract

Metal additive manufacturing (AM) is constantly developing and expanding into new segments. The automotive industry has so far not implemented AM to any larger extent. One reason is the relatively high cost of AM-components, but mainly due to the materials that are available is not used to a larger extent within the automotive sector e.g. titanium and stainless steel. Powder Bed Fusion–Laser Beam (PBF–LB), the most developed metal AM-method had, until recently, a limited range of materials available.
However, recently several low-alloyed carbon-containing steels, that are commonly used in vehicles and machined components have been developed. One issue with increased carbon content is that the material has shown to be difficult to manufacture with PBF–LB. Moreover, heat treatment and its influence on residual stresses, microstructure and hardness are not yet known.
This thesis focuses on the residual stresses and how they are affected by the heat treatment on samples printed in a low alloy medium carbon steel, 42CrMo4 (AISI 4140). The heat treatments applied in this thesis were not intended to be optimised for 42CrMo4, but rather investigate a more industrial approach using relatively standard heat treatment cycles. After analysing the different heat treated samples it was found that in a regular quench and temper cycle, the parts achieved similar hardness as conventionally manufactured 42CrMo4 using the same heat treatment. Samples exposed to a direct temper cycle, hence just tempered as-printed, showed promising results in terms of residual stresses. This knowledge may serve as a basis to further research and development of heat treatment cycles to better utilise 42CrMo4 steels in the automotive sector.

Keywords: Additive Manufacturing, Heat treatment, SEM, XRD, Microstructure, 42CrMo4, AISI 4140, PBF-LB, Residual stresses.

Acknowledgements

I would first of all like to give a big thank you my supervisors Henrik and Rasha for their continuous support during the thesis. Especially to Henrik for being a sounding board for many of my questions and conundrums I faced, and to Dinesh and Rasha for all the great help during the XRD work. I would like too reach out and give my thanks to everyone at Volvo Materials Technologies for their support with my experiments and and different inquiries. I would also like to give my thanks to Arvin and Erik at Bodycote for the help with the heat treatment of the samples, and to Peter Harlin at Sandvik for great discussions and tips. Finally I would like to direct a huge thank you to my friends and family for believing in me, and their support during my years at Chalmers University of Technology and the thesis work.

Rasmus Kristensen, Gothenburg, January 2024

List of Acronyms

Below is the list of acronyms that have been used throughout this thesis listed in alphabetical order:

AM	Additive Manufacturing
DMLS	Direct Metal Laser Sintering
EBSD	Electron Backscatter Diffraction
EDS	Energy-Dispersive X-ray Spectroscopy
HK	Knoop hardness
HV	Vickers hardness
NDT	Non-Destructive Testing
OM	Optical Microscopy
PBF-EB	Powder Bed Fusion - Electron Beam
PBF-LB	Powder Bed Fusion - Laser Beam
Q&T	Quench & Temper
SEM	Scanning Electron Microscope
SLM	Selective Laser Melting
XRD	X-ray Diffraction

Contents

List of Figures

List of Tables

1
Introduction

This Master Thesis was executed at Volvo Group Truck Technology – Materials Technology in Lundby, Gothenburg. This chapter will briefly describe Volvo, give a background to the thesis, forward a problem statement and describe the scope, as well the constraints, of the thesis work.

1.1 Volvo Group Truck Technology

Volvo Truck Technology (Volvo GTT) is a part of Volvo AB. Volvo was founded during the 1920s with the first Volvo car, ÖV4, produced in 1927 and the first Volvo truck, Series 1, in 1928, of which both were built on the same production line. Volvo GTT is responsible for the engine development, technology research, prototype construction, product design and all the technology and product development linked to the truck development, as well as providing support in the aftermarket for the vehicles.

Volvo Group Trucks is a world leading truck manufacturer known for producing well built, powerful and versatile trucks for a variety of different tasks. Volvo Group has over 100.000 employees world wide, production facilities in 18 countries and a presence in 190 markets. Volvo Group encompasses not only Volvo Trucks, but also Volvo Penta, Volvo Buses, Volvo Construction Equipment, Mack Trucks and Renault Trucks among others. The main product development and prototype production/testing is placed at Lundby, Gothenburg.

Volvo Materials Technology is providing support to all branches within the Volvo Group and performs material testing for past, present and future technologies.

1.2 Background

Additive manufacturing (AM), the technique of producing parts by adding material layer by layer, has the capability of producing complex geometries that can not be achieved with conventional machining techniques. This has opened up opportunities to produce parts thought to be nearly impossible or very expensive to produce [1]. These capabilities have made AM very popular within the medical industry among others, since many implants are unique and often needs custom fitting; in such applications AM excels compared to conventional machining, with a lower price per part for small batches and the possibility to produce parts on demand when it is needed with reduced lead time [2]. The possibility to produce small batches

on demand for custom applications, e.g aftermarket parts, is a clear advantage compared to other manufacturing techniques.

AM has also enabled the use of new materials in new areas with the help of different AM techniques such as material jetting, direct energy deposition, VAT photopolymerisation and powder bed fusion. The material development has not only been on metals but also polymers, shape memory alloys and even composites [3]. Concerning metal AM and PBF-LB, the main development has been around stainless steels, nickel based alloys, and aluminium, whereas little has been done on low alloy steels. Approximately 40 different metallic materials are to this day approved for use in PBF-LB [4]. Low–alloy carbon–steels, is a big part of the materials used for the automotive and construction industry, mainly because of the excellent properties concerning wear resistance, toughness, strength and relatively low cost [4]. The wide range of adaptability comes from the possibilities to heat treat and change the steels characteristics for a specific application.

Heat treatment of steels has been applied as long ago as 900 BC where Egyptians found that quenching the hot steel in water greatly improved the sharpness and hardness of swords and knives [5]. A deeper understanding of the hardening process began in the start of the 20^{th} century by gentlemen such as Adolf Marten (martensite) and Robert Austen (austenite) [6]. Today every piece of steel is in some way heat treated, and in 2010 the whole heat treatment market value was estimated for Europe to a value of around 10 billion euro, it is also estimated that the automotive industry stands for 60% of all the heat treatments done directly and indirectly [6]. Without heat treatment or hardening it is most certain that products such as screwdrivers, cars, razors, made out of, or containing, steel would have a significant lower life time and also being significant heavier.

Additive manufacturing have recently gone from being a way to produce prototypes and test ideas, to real production of small series for end usage. The development of the technique enables rapid on demand production for parts, it can also introduce new materials to the automotive industry. This is why Volvo GTT is pursuing research of heat treatment of low–alloy steels in additive manufacturing. Scouting the possibility to introduce AM parts in to their industrial infrastructure, with research on how different heat treatment steps affect the properties and microstructure of the produced parts.

1.3 Purpose

The purpose of this project is to give a deeper understanding of the heat treatment of parts made of the low alloy steel 42CrMo4 (AISI 4140) with PBF-LB. By using a cost-efficient heat treatment of the material, its introduction into the automotive industry would be facilitated. Moreover, the project aims to create a deeper understanding of which heat treatments are suitable for additive manufacturing of 42CrMo4. Also,

the influence of heat treatment on the printed parts and the behaviour of the microstructure, hardness and residual stresses will be analysed.

Research questions

RQ1: What is the response of additively manufactured 42CrMo4 to various heat treatments?

RQ2: What is the distribution of residual stresses in additively manufactured 42CrMo4, in as-printed and heat treated condition?

RQ3: How does the hardness of additiviely manufactured 42CrMo4 compares to conventionally manufactured one after various heat treatments?

1.4 Limitations

This project will not discuss the environmental or political aspects of production, nor the energy- and production efficiency of additive manufacturing and heat treatment. The project will neither look in to the mining of material or the production of powder for the additive process. The thesis will not treat post-processes for the types of AM as; Powder Bed Fusion - Electron Beam (PBF-EB), VAT Photopolymerzation (VPP), Fused Deposition Modeling (FDM), Binder Jetting (BJT), Direct Energy Deposition (DED) and Sheet Lamination (SHL). It will neither go too deep into the techniques of heat treatment, only cover how they work and influence the properties of the printed metal parts. The hardness values compared towards will only be from publicised data rather than personal tests.

2
Theory

This chapter will go through the most vital theory that lay the foundation for this thesis, to give some understanding of the general techniques and the essential knowledge to understand the work that has been done.

2.1 Low-alloy steels

Low-alloy steels are a broad family of steels that are among the most used steels in automotive and construction applications. These are steels with a total alloy content of 2 wt% in the low end, up to a content just below the levels of a stainless steel that contains a minimum of 10 wt% Cr.[7] Other requirements for the steel to be low-alloy are that the alloying content does not exceed 1.65% for Mn, 0.60% Si and 0.60% Cu [8]. Low-alloy steels can be further categorised depending on carbon content, <0.30wt% C are called low-alloy low-carbon steels. Steels with a carbon content between 0.30–0.60wt% C are called low-alloy medium carbon steels. The last category is the low-alloy high-carbon steels, with a carbon content of 0.60–1.00wt% C [9].

Low-alloy medium-carbon steels have excellent properties regarding hardenability, which is one of the reasons why it is a popular choice in structural and automotive components, alongside its versatility and relatively low cost. It is also common in general engineering applications [10][11], due to its great properties, high strength, toughness [12] and good machinability [13].

42CrMo4

42CrMo4 (American grade: AISI 4140), is a low–alloy medium-carbon steel. The components where 42CrMo4 is used include crankshafts, gears, bolt assemblies, among others. The alloying elements within 42CrMo4 all have an important role to improve the mechanical, chemical and physical properties of the alloy. The following is a list of the alloying elements present in 42CrMo4 and a short description of the impact they have [4][14][15][16]:

- **Carbon:** The single most important alloying element in steels. Increases strength and hardness, stabilises austenite and is essential to form perlite, martensite, carbides, cementite and bainite.
- **Silicon:** Added to limit the oxidation and improve strength in a quenched and tempered state. Also to prevent carbide growth during tempering over long periods of time.

- **Manganese:** Added to increase hardenability, stabilising austenite, promote carbide formation and form non-harmful sulphides. It has an disadvantage of being a strong oxide former.
- **Phosphorus:** Added to stabilise ferrite formation, shown to inhibit temper embrittlement with increased content and give a strong solid solution hardening.
- **Sulphur:** Added to increase notch impact toughness and improve machinability. Weldability is however decreased with increased sulphur content.
- **Chromium:** Added generally to improve corrosion resistance, but also hardenability, high temperature strength and to promote carbide formation.
- **Molybdenum:** Added to increase hardenability, inhibit temper embrittlement and increase high temperature creep and tensile strength. To inhibit embrittlement it has to be an specific amount alloyed, between 0.15 and 0.30%.

2.2 Powder Bed Fusion - Laser Beam (PBF-LB)

PBF is the most prevalent and used AM technique to manufacture metals with AM, the two most common PBF techniques are the ones using Electron Beam (EB) and Laser Beam (LB) as an energy source to melt the metal [17]. LB is the technique used to print the samples used for this thesis.

In PBF-LB (also known as SLM/DMLS) the part is printed on a powder bed within a chamber, under (most often) inert gas, such as argon or nitrogen, to shield the metal from oxidising during melting/solidification [18]. The laser beam, with help from mirrors for re-directing, scans the powder bed and selectively melts the powder according to a CAD-model. The CAD-model of the part has been imported to a slicer program that slices the model into 2D-layers for the printer to read and melt the powder layer accordingly. When the layer is finished, a piston holding the powder bed is lowered a minuscule amount followed by a re-coater sweeping or rolling new powder, from another bed next to the powder bed, to coat the bed with powder for the next layer and the scanning process starts again. If there is too much powder in front of the re-coater it will be collected in the collector bin to be reused. This repeats layer-by-layer until the part is finished. The end result is a powder cake that needs to be removed for the parts to be visible, and thereafter the parts needs to be cut from the build plate. Figure 2.1 illustrates the whole process. [4][19]

Metal powder

The powder used in the PBF-LB can be virgin or re-used, though depending on how many times it has been re-used the production parameters may need to be changed since virgin powder is free of possible contaminants from earlier production. Contaminants can be oxides or sputter. The production of the powder is typically performed by gas atomisation. The metal is in a liquid state, and a small stream is guided into a pressurised chamber. The stream enters the chamber through a nozzle, there the droplets are blasted with inert gas to atomise and solidify into small powder particles. The powder is then collected in the bottom of the chamber.

The most commonly used atomising process is gas atomisation, since it is a great technique to control the size of the powder particles and into a favourable spherical shape. [20][4]

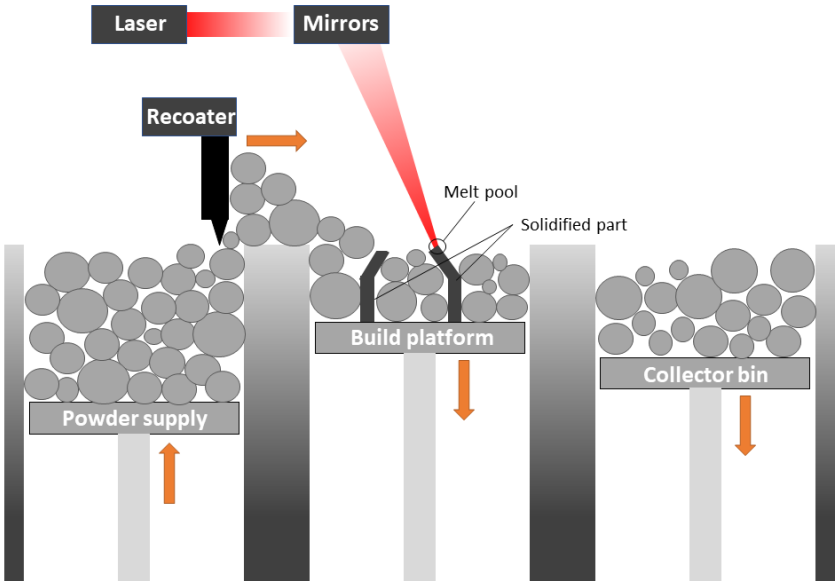

Figure 2.1: Schematic illustration of the PBF-LB process, redrawn from [4]

2.3 Heat treatment

The heat treatment is a core function to adapt the steel towards each use case for optimal performance. Heat treatment of metals and for most steels has been done for centuries to optimise the performance of steel. From making swords stronger and lighter, more notably within the 'Damascus swords' during the medieval period [21], to heat treat crankshafts using case hardening to make them stronger and lighter within combustion engines. The heat treatment is performed essentially to alter and adapt the steels properties to each use case through such as hardening, annealing, normalising and nitriding. The choice depends on how the part is produced, e.g forged, pressed and sintered, cast etc. The choice also depends on what the goal for the part is, for example if it is to achieve higher tensile or fatigue strength, wear resistant surface, good machinability etc. The cost is a big factor as well, since some heat treatments are more costly than others, see Figure 2.2 for the most common heat treatments used depending on desired characteristics.[6]

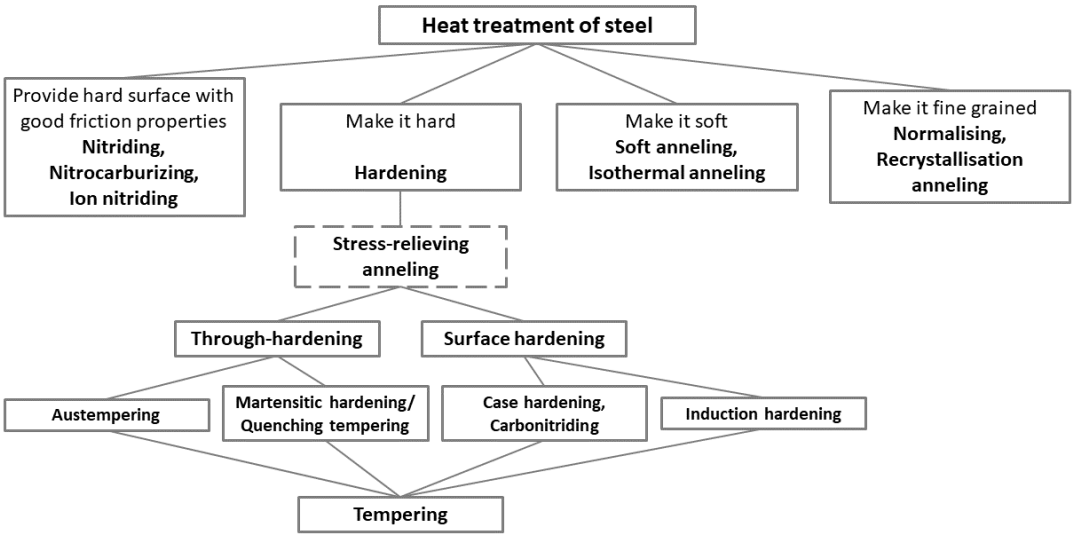

Figure 2.2: Schematic of the most common heat treatments, redrawn from [6].

Hardening

One of the most common heat treatments, and also as previously mentioned, the oldest technique is the art of hardening steel. It is performed by heating the steel up to a austenization temperature, for carbon steels it ranges from approx. 723°C up to 1392°C depending on alloying- and carbon content [22]. Realistically heating over 950–1000°C is redundant, since most alloys and carbides will diffuse if left at chosen temp for a set hold time. For low–alloy steels the carbides will dissolve easily and only a hold time of 5–15 min is required, for medium-alloy steels it is around 15–20 min. The temperature may be adjusted to shorter or longer times depending on the geometry of the part. [8] It is also advantageous to austenize at as low temperature as possible due to the grain growth at higher temperatures. Larger grains will lead to a more brittle material due to low number of grain boundaries to stop dislocations.

For 42CrMo4 the austinization temperature ranges between 840 – 880°C [23]. This is a temperature range where the carbon and all other alloy elements diffuse and recrystallise. This is advantageous to do since it is normalising the steel into a state where one can tailor the steel via cooling the steel at different speeds, see Appendix A.1 and A.2 for CCT and TTT-diagrams (simulated by using J-MatPro). When austenitized, the steel is quenched in oil or other cooling medium such as water for faster cooling. The oil is heated to a temperature of 80°C to minimise the vapour-jacket that is formed if the quench medium is too cold. Thus the rapid cooling that is desired to form martensite is prolonged and other possible phases are formed.

Hardening is followed up with tempering when the goal is to add more toughness to the steel. Tempering removes the extreme brittleness that hardened steel has after quenching to be able to use the steel. Tempering a steel performed by reheating the

part in the furnace, slowly increasing the temperature to the set temp which usually is around 100–300°C for steel. Then the parts are held at the set temperature for a set time, normally for steels 1–2 hours, sometimes longer depending on which traits is wanted from the steel. The longer time in the oven the more ductile the steel becomes. After tempering the steel the oven is turned of and the steel is left to cool inside with the furnace, or taken out from the furnace to air cool. [6][24]

Temper embrittlement

Tempering is as previously described a method to increase the toughness in hardened steels, however it can cause embrittlement if done incorrectly. Temper embrittlement is a phenomenon occuring when tempering steels in temperatures between 250°C–600°C. The brittleness occurs due to a number of different metallographic phenomenas at different temperatures. [6]

At the temperature range 250°C–400°C (called 350°C embrittlement) phosphorus (P) has an serious impact on the steel after hardening, dividing the grain boundaries during the austenitization and causing carbides to grow at the grain boundaries when tempered in the interval. This is prevalent in low-alloy and most non-alloyed steels. [6][16]

In the temperature interval 375°C–575°C the embrittlement occurs on quenched & tempered alloys regardless of phosphorus content and is rather dependent on tempering time and temperature. It can become a problem when cooling slowly over the temperature interval from heat treatment, especially when tempering over relative long time periods. The embrittlement caused by this temperature interval can be reverted by heating to, or over, 575°C, effectively restoring the alloy. [6][16][24]

2.4 Residual stresses

Residual stresses are defined as stresses that are retained in a body without any external forces affecting the body, left from processes such as manufacturing, welding and heating [25]. There are different classifications of the residual stresses depending at which scale they operate. Type I stresses are macro-stresses that affect the entire body or part, type II stresses are micro-stresses that act at a grain scale level and last type III stresses that are nano-stresses affecting on a atomic-level [26]. For parts produced with PBF–LB the focus has generally been on Type I stresses due to the stresses approaching the yield stresses, leading to parts being deformed and cracked. [25][27]

Residual stresses of Type I (or global residual stresses) are caused by non-uniform deformation, much like bending a beam past the elastic point and causing permanent deformation on the beam and residual stresses arise when the load is let off. Thermal loads affect residual stresses in the same way, as when a part is being quenched, the material close to the edge of the body is cooled faster than the inside. Thus the outer material is contracting due to the colder quenchant and the warmer inside of the body restricts movement, causing residual stresses to form. [25]

Welding affects the body much like quenching, however here the body is heated locally which causes the metal to expand and cause plastic strain in the weld and regions near the weld. When the weld cools it causes local shrinkage and distortion, which causes residual stresses to form [26]. Similar to how residual stresses are formed during PBF–LB. When a new layer of powder is deposited and melted on the previous layer, a large temperature gradient is formed due to slow heat conduction to the layers below. Causing the top layers to form a compressive force due to expansion and the layer below ends up in tension. When cooling the melt pool contracts and solidifies causing a tensile force. The layers below restrict the movement of the top layer and thus ends up in a compressive state, see Figure 2.3.

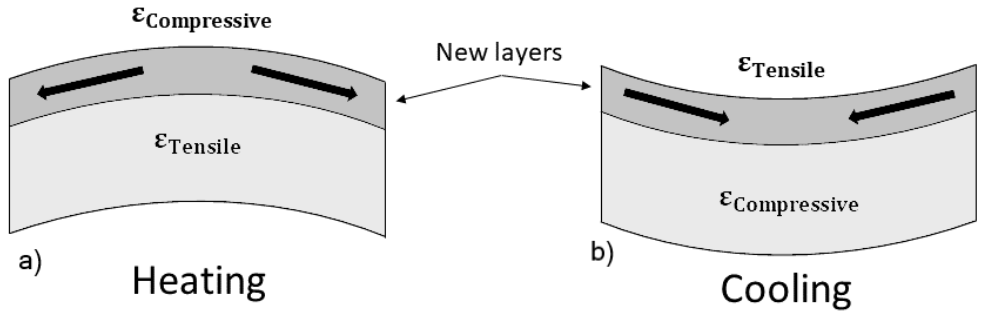

Figure 2.3: Schematic illustration of residual stresses induced by PBF–LB during melting of the powder, a), and cooling of the solidified metal, b). Redrawn from [4][25].

X-ray Diffraction Analysis

With X-ray Diffraction (XRD)-analysis the residual stresses can be measured within a sample/test piece. Though stress is not really measurable as the term "stress measurement" might give appearance to. Stress is more of a extrinsic property and to measure, or determine, stress it is required to measure some intrinsic property as area and force or strain, and calculations of the stress [28]. To measure residual stress one need to use Bragg's Law, where the distance in between the lattice and the distance d is measured, and then calculate the resulted residual stress. To measure the stress using XRD it is assumed that the crystalline lattice elastic distortion behaves linearly. It is also required to have a relatively fine grained material and a relatively smooth surface since the XRD only can penetrate to a maximum depth of 10 µm[1].

One could physically measure stress via mechanical methods such as hole drilling, where a strain gauge is installed on the surface and a hole is drilled close to it. The residual stresses are measured via the relaxation of the material when the hole is drilled, but they are destructive and limited to the sample size and geometry. [26][29]

[1]Specific for the equipment at hand during the thesis

Bragg's Law

The main principle that makes XRD analysis possible is Bragg's Law, discovered by W.L. Bragg in the early 19th century. Bragg theorised and showed that diffracted X-rays deflect and bounce from planes within crystals. These planes are the rows of atoms in what makes up a crystal structure, see Figure 2.4. [30]

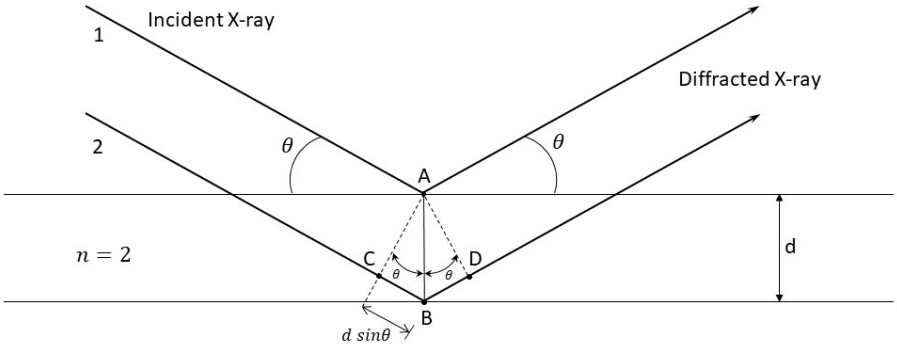

Figure 2.4: Illustration of Bragg diffraction, redrawn from [28][30].

X-ray wave 1 and 2 are in the same phase towards the specimen and reflect from Atom A and B in a crystal with the atomic plane separation distance, d, defined as

$$d = \frac{a}{\sqrt{h^2 + k^2 + l^2}} \tag{2.1}$$

The a is the lattice spacing of cubic crystal and h, k and l is the Miller indices of the Bragg plane. The reflection angle, θ, of the diffracted x-rays is the same as the angle of incidence, θ. The condition for the two waves to stay in phase with each other after being reflected is that the combined length of the distance between point, C, B & D, is a whole number, n, of wave lengths, λ. The distance CB and BD are equal and to $d * sin\theta$, thus

$$n\lambda = 2d * sin\theta \tag{2.2}$$

which is Bragg's Law. In Figure 2.4, n is equal to 2 (second order) which is a whole wave length between CB. With a higher number for n the reflective angle, θ, would be larger e.g 3 (third order). If the angle would correspond so n would not be a whole number, the waves will not be in phase and cancel each other out through destructive interference. Combining equation 2.1 and 2.2 results in

$$\left(\frac{\lambda}{2a}\right)^2 = \left(\frac{\lambda}{2a}\right)^2 \frac{1}{\sqrt{h^2 + k^2 + l^2}} \tag{2.3}$$

With equation 2.3 one can derive the selections rules of which Miller indices for different cubic structures are viable, e.g BCC structure $h + k + l =$ even. [30][31][32]

Principle of XRD

Figure 2.5 illustrates the diffraction of a X-ray beam, **S**, at a general specimen. The diffraction angle, 2θ, in this instance is relatively high towards the specimen and measures the stress in two different angles relative to the normal, **N**, of the sample surface. Ψ in (b), defines the angle between the normal of the sample surface and the incidence/diffraction point. As stated in section 2.4 the diffraction happens at an angle of 2θ, see Figure 2.5. In Figure 2.5 one can also see the influence of taking stress measurements in different angles towards the normal of the specimen.

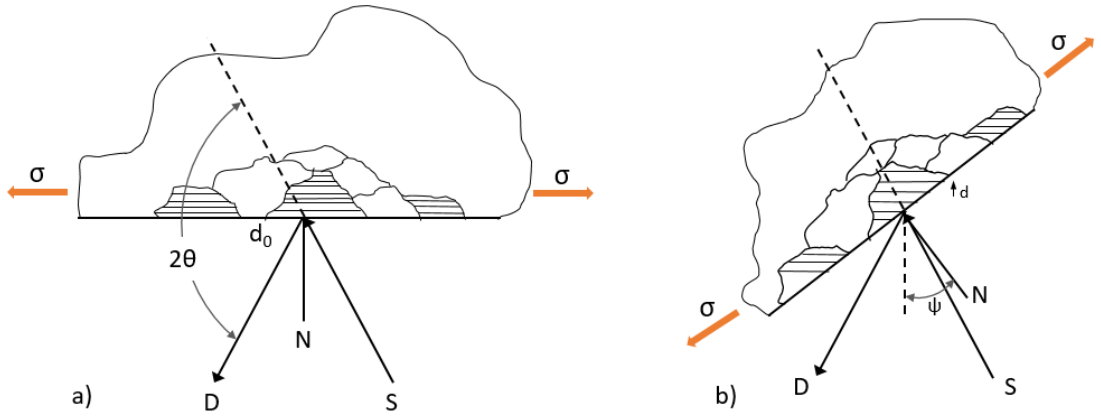

Figure 2.5: Principles of XRD residual stress measurements. **D**, X-ray detector; **S**, X-ray source; **N**, normal to the surface. (a) $\Psi = 0$: Poisson's ratio contradiction of lattice spacing. (b) $\Psi > 0$: Tensile extension of lattice plane by stress σ.
Figure redrawn and descriptive text cited from [28].

As seen in Figure 2.5a, the only crystals within the sample that satisfies Bragg's law and diffract the x-rays are the ones parallel to the surface. If there is a presence of tensile (or compressive) as the case of Figure 2.5, the Poison's ratio slightly results in a contraction and reducing the lattice spacing of the crystals within the sample. When the sample is tilted to a known angle ψ, as in Figure 2.5b, the crystals that now are parallel had their lattice spacing increased to a more relaxed state. Measuring the change of the diffraction peak in at least two different angle makes it possible to calculate the stresses present within the samples. this is why it is beneficial to measure in multiple angles to get an accurate reading of the stresses present. Due to the changes of the mean lattice spacing, only elastic strains are measured with the XRD, when the elastic limit is reached it results in dislocations which disrupt the crystal lattice and the formation of micro-stresses. [28]

Residual stress, depth profiling

Analysing the samples via depth profiling is necessary to understand the effect of the heat treatment, and in a as-printed state, on stresses, as the x-rays cannot penetrate that deep into the specimen [33]. Since the radiation that is suitable for XRD is quite "kind" with a low amount of energy put into the specimen, usually around 5 to 8 keV. Electropolishing is used to remove the material layer by layer, exposing new surfaces for subsurface measurements. This is performed without introducing any new stresses, plastic or thermal, to the specimen and distorting the measurements. [34][35]

2.5 Sample preparation

The sample preparation is of outmost importance to give a good chance at accurate results in later steps during the analysis of the parts. The sample preparation consists of several steps:

1. Cutting
2. Mounting
3. Polishing
4. Etching

Cutting

The raw specimen is cut into more manageable pieces, using an abrasive cutter, prior mounting for subsequent analysis (e.g. microstructure and microhardness). There are cutting wheels of both abrasive wheels and diamond tipped wheels, the abrasive wheels are cooled with cutting fluid to not heat up the specimen and possibly change the properties. The downside with the use of cutting fluid is that it contaminates the surface of the specimen and will give inaccurate readings and possibly destroy the kind of information one wants to find when cutting open a sample. The diamond tipped wheels has no need for cutting fluid since they operate with lower speeds $<$300 rpm.[36]

Mounting

When the area of interest is exposed, the piece is most likely in an awkward shape so mounting it in a puck of resin is preferable for further analysis. The choice of mounting material is important, for this application a resin that is grindable and able to transfer current is preferable. Since the specimens will be polished to accurately analyse the surface and also lead current since the specimens will be analysed with the SEM. [36]

Grinding/Polishing

After the mounting of the specimens to a puck the surface is still rough due to the cutting step, this is where grinding and polishing of the specimens comes in. Grinding is roughly the same as abrasive cutting, the tools consists of particles cemented together to form a cutting wheel or an abrasive lap stone. In some cases the abrasive particles are cemented on cloths or paper to create consumable abrasive paper, belts and cloths. The risk of grinding is to introduce heat to the piece, same as in abrasive cutting, and thus hardening the surface, therefore grinding is done in small steps moving slow between grits (coarseness of the grind paper/stone) and in some cases using cutting fluid to prevent that from happening. [36]

Polishing also uses abrasive particles, however they are not fixed on a wheel or a paper back. They are rather suspended in a liquid or a paste and then polished with a cloth or a cloth wheel to provide a mirror like finish. [36]

Etching

Etching is performed to reveal the microstructure of the specimens, since on as-polished surface it is hard to distinguish the microstructure on the specimen. Pores, cracks, pits and non-metallic inclusions may be visible without etching. The etchant is a solution that chemically attacks the polished specimen and can be a variety of different solutions such as: Nital 1-3%, aqua regia, diluted nitric acid and sodium thiosulfate. In this thesis Nital will mainly be used, since this is the most common etchant used to reveal the microstructure of steels. There are also dry etchants as well but nothing that will be used within this thesis. [36] Often etching is done after the hardness analysis since the indents are easier to analyse when the samples are un-etched.

2.6 Hardness test

Vickers

The hardness of a specimen can be measured with a number of different techniques such as Rockwell (HRC), Brinell (BHN), Knoop (HK) and Vickers (HV). Vickers and Knoop will be used as the testing methods in this thesis. Vickers is performed via pressing a tetrahedon shaped tip into the specimen with a specialised load. The facets have an angle of 136°±0.5°. A set force is applied with the tip forming a permanent mark on the specimen that is later measured diagonally across the indent (d1 and d2), from there the specimens hardness can be decided, see Figure 2.6. [6][37] To calculate the hardness the following equations is used:

$$HV = \frac{F}{A} \cong 1,854\frac{F}{d^2} \tag{2.4}$$

There F is the force applied and d is the average sum of the two diagonals of the indent in mm, the coefficient 1,854 is for the geometry of the indenter.

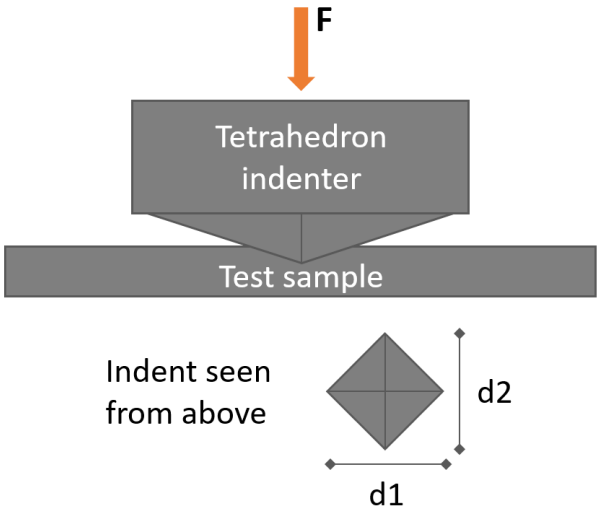

Figure 2.6: Illustration of Vickers indent, redrawn from [37].

Knoop

Hardness testing with Knoop is very similar to Vickers; there, the only difference is the tetrahedral tip is in a rhombus shape. There the longer diagonal is seven times longer than the shorter one, making the angles larger than the Vickers indenter. The angle for the longer diagonal is 172.5° and the shorter diagonal 130°. The indent becomes shallower than the Vickers indent at the same force applied, making it exceptional to measure hardness in brittle materials, close to the surface and/or placing the indents tight together [6][38][39]. To calculate the hardness the following equations is used:

$$HK = \frac{F}{A} \cong 14.299\frac{F}{d^2} \tag{2.5}$$

There F is the applied force, d is the length of the longer diagonal in mm and 14.229 is coefficient for the geometry of the indenter.

3
Materials & Methods

In this chapter the materials used, as well as the different methods applied and different techniques will be described, such as residual stress measurements, microscopy, among others.

3.1 Material

The samples for this project were provided by the Competence Centre for Additive Manufacture - Metal (CAM2), hosted by Chalmers University of Technology and William Hearn. These samples were printed using an EOS M290 printer with the parameters specified in Table 3.1. The striped laser pattern for each powder layer was rotated by 67°. The material used for printing these samples is a 42CrMo4 steel powder provided by Sandvik Osprey^{TM}, the chemical composition of the powder is seen in Table 3.2. The size of the powder particles was sieved to a size range of 15–45 µm. [4]

Table 3.1: Printing parameters for the EOS M290 when manufacturing the samples [4]

Layer thickness	Hatch spacing	Laser power	Scan speed	Preheating temperature
20 µm	70 µm	170 W	1011 mm/s	180°

Table 3.2: Chemical composition of the 42CrMo4 powder, provided and supplied by Sandvik Osprey^{TM}[4]

C	Cr	Mo	Mn	Si
0.38–0.47	1.0–1.1	0.20–0.23	0.60–0.77	0.20–0.29

To confirm the chemical composition of the samples, one sample was sent to Volvo's chemical lab in Skövde for examination. More details can be found in Section 3.3. Another sample, in as-printed condition as well, was sent to Volvo's measurement lab to measure the surface roughness according to SS–ISO 4287 and ISO 11652.

The samples serve as injector yokes, which are used to secure the diesel injectors in a Volvo Penta TAM72A engine, among other engines. Previously, the yokes were manufactured through press sintering and later switched to a machined part. Now, it is being explored to possibly producing them as a AM parts, see Figure 3.1.

Figure 3.1: Sample of the yoke, printed with PBF-LB

Heat treatment

The heat treatment in this thesis is not aimed to be optimised for 42CrMo4 printed using PBF-LB, rather a more industrial approach to simulate the use case of the parts in real usage. Therefore, commercial Quench and Temper (Q&T) operations were used.

All the printed samples received a specific number engraved to the piece to simplify identification during testing. This number corresponded to Table 3.3 which described what kind of heat treatment the specific sample received. The heat treatment was done at Bodycote, a company specialised on heat treating and surface coatings that, based in Angered. This was done so the results of the residual stress measurements and microscopy would not be compromised. The different temperatures was decided by analysing the general guidelines and what different manufacturers and researchers recommend, to set a baseline and something to compare against.[6][23]

Table 3.3: The different heat treatments done to all of the samples

Sample nr.	Heat treatment	Aust.temp[°C]	Tempering[°C]	Quench/Cooling
#1	”As printed”	x	x	x/x
#2	Direct Temper	x	200, 1h	x/Air
#3	Direct Temper	x	650, 1h	x/Air
#4	Quench & Temper	840	200, 1h	Oil/Air
#5	Quench & Temper	840	650, 1h	Oil/Air
#6	Quench & Temper	840	200, 2h	Oil/Air
#7	Quench & Temper	840	650, 2h	Oil/Air

The samples that was Q&T were heated up to 840°C in 15 min and held there for one hour and subsequently quenched in oil held at 80°C. After the quench, the samples were tempered at 200°C or 650°C for one or two hours. After the tempering stage the samples was left to air cool. No protective gas was used during the tempering. To simulate the case of treating the pieces with other regular steel that is not produced by AM.

3.2 Residual Stress Measurements

The first part of the stress measurements was on a selected number of points on the surface of the samples, the specific points was decided from analysing previous test reports from Volvo Materials Technology [40] where the components break during excessive loads, see Figure 3.2a and 3.2b. The fractures occurred along the side of the through-hole for the mounting screw and the ”fingers” of the yoke.

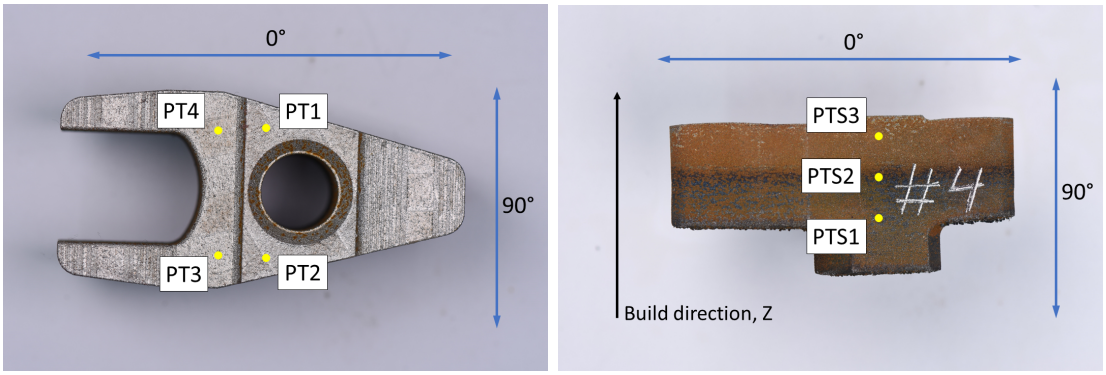

(a) Measurement points on the mount (top) side

(b) Measurement points on the side of the sample

Figure 3.2: Points for the surface residual stress measurements

The stresses were measured in two different angles perpendicular to each other, to see possible deviations from the melt pattern of the PBF-LB. This is especially interesting when analysing the side of the samples, measuring stresses along and transverse to the build layers since this is where Hearn et al. [4] found cracks to be formed. The set-up of the XRD[1] was as shown in Table 3.4,

Table 3.4: Settings for the XRD when analysing the residual stresses on the surface

2θ	Collimator [mm]	Exposure time [s]	Oscillations	Angles [°]
211	3	10[2]	5	12 (-40° to 40°)

Depth Profile

The depth profiling is performed in a similar manner as the regular stress measurements described in section 3.2; the same settings for the XRD is also applied shown in Table 3.4. The depth profile is performed on one specific spot on the sample, namely PTS2, see Figure 3.2b. This area is where cracks and failures were observed when the previous yokes were tested (sintered parts) [40].

[1] Stresstech Xstress G3

[2] At some points on some samples, the exposure time had to be increased due to poor intensity of the peaks

When performing a depth profile the working order is as follows:

1. Measure the stress on a point on the sample
2. Electropolish the point that the measurement was taken
3. Measure the depth of the electropolished surface with a micrometer
4. Repeat the order from the first point

The electropolish is done in increments controlled by a set time on the electropolisher. Shorter time has better control, electropolishing for a longer time means that more material is removed and it is easier to miss the target. Since it is near impossible to hit a specific depth within a micrometer, 10 measurements are taken on the same point and a average of all is taken. There are some depths that are aimed for, if the depth was found to be too far off target a new series of polishing was done and the depth was re-measured. But the target depth will most certainly not be hit, yet likely close enough. Since all the points are noted and put on a stress/depth curve to analyse the influence of residual stress through the surface layers. For the electropolishing a Struers Movi-Pol 5 was used, with perchloric acid ($HClO_4$) diluted with an electrolyte as etchant. To measure the depth after each polish, a calibrated Mitutoyo micrometer was used together with a custom 3D-printed holder for the samples. Since the geometry are not favourable to place the samples directly on the measure plate, a holder for the samples was designed and 3D-printed in PLA with a Ultimaker 3 Extended, so the measurements can be done in as a reliable and repeatable manner as possible, see Figure 3.3.

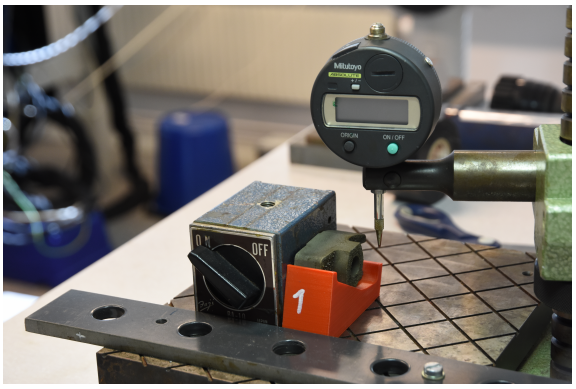

Figure 3.3: Setup to repeatably hold the yoke in the same position when using a plunger type micrometer to measure the amount of material removed.

The depths aimed for during the electropolishing is presented in Table 3.5, and settings for the polishing are presented in Table 3.6

Table 3.5: Depths aimed for when polishing the samples.

Depth [μm]	20	50	100	150	200	250

Table 3.6: Settings on the elecropolisher when performing the depth profiles.

Electrolyte	Voltage	Flow	Time
A2 (Perchloric acid)	45 V	8	Varies

3.3 Sample preparation

When the depth profiling of the samples are finished, they are to be cut open to expose the microstructure for further analyses, such as microstructural analysis and micro hardness measurements.

The samples were cut with a abrasive cutter, at a reasonable low cutting speed with cutting fluid to reduce the amount of heat in the samples. The samples were cut into two main pieces, see Figure 3.4. One off-cut of Sample #1 (As-printed) was sent to Volvo's own chemical lab in Skövde for a chemical analysis of the composition in the yokes. After sectioning the pieces they were moulded in a non-conductive thermoset resin and polished in several steps resulting in a mirror like finish.

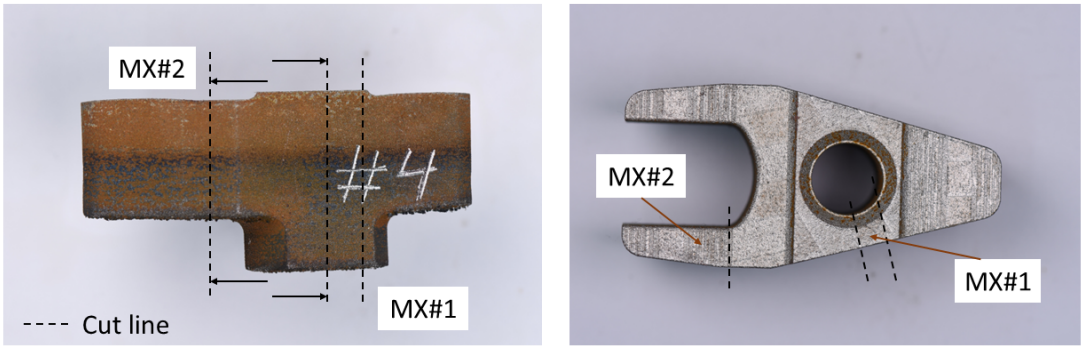

Figure 3.4: Illustration of where the cuts been placed and which surfaces being examined.

The samples were denoted accordingly, e.g for Sample #2 (Direct Tempered at 200°C), M2#1 for the sample cut from the through-hole and moulded in a resin puck and M2#2 for the sample cut from the fork of the yoke and moulden into a resin puck, see Appendix D for a detailed denotation.

3.4 Optical Microscopy

When the samples had been cut, mounted and polished the 14 micro samples were examined in a inverted optical microscope[3] (OM) before etching, see Figure 3.5. This revealed possible cracks, inclusion, porosities and lack of fusion in the samples. Afterwards when they been examined un-etched, the samples was etched in a 1%-3% Nital solution to bring forward the microstructure of the samples, and later being examined with the same inverted OM in order to analyse the microstructure.

[3]Leica DMI 5000 M

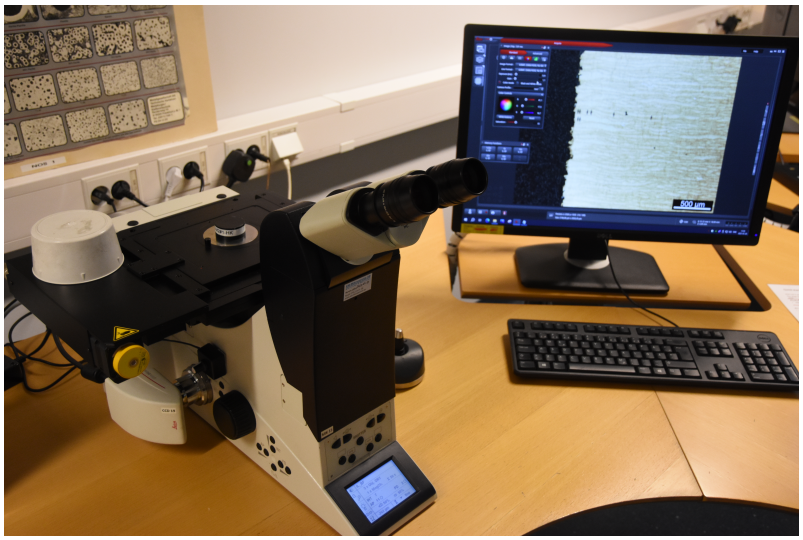

Figure 3.5: One of the samples being examined in the inverted OM

3.5 Hardness measurement

In between the two microscopic analyses several hardness profiles were performed on all the samples to get an idea of how the heat treatments affected the samples in terms of hardness (and possible de-carburization). A Struers DuraScan 70 was used to set up and perform the profiles. Six samples were put in a holder at the same time, see Figure 3.6a. The software allowed to set up multiple profiles after each other. Four profiles per sample were performed, one from the top (mount) surface, one on each side in the middle (inside and outside) of the sample and one from the bottom (start layers of the build), see Figure 3.6b.

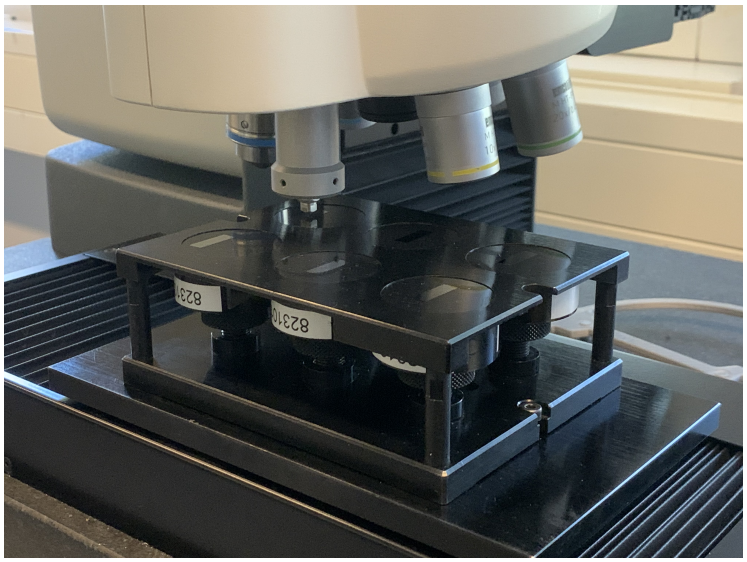

(a)

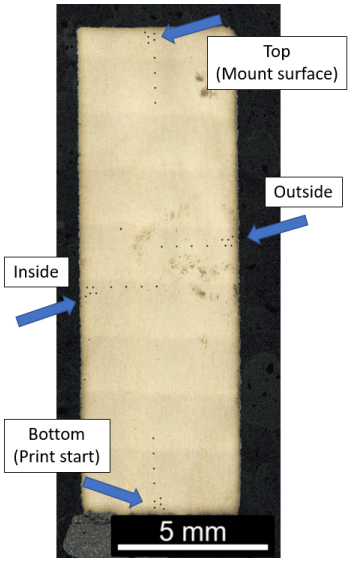

(b)

Figure 3.6: **(a)** Six samples set up for hardness profiles and in **(b)** Etched, Sample 5 fork (M5#2), there the indents from the hardness profiles are visible

The indents were set apart in an offset patter so the indents could be spaced in 100 µm increments in depth. The load used to on all profiles was 0.5kg. The reason to offset the indents is to get as much of the surface profile as possible. Because of deformation of the material, the indents are to be spaced apart 3x the length of the diagonal of the indent, e.g if one is expecting a 50 µm indent the indents need to me at least be 150 µm apart. So if the indents are set in a straight line a great deal of information about the hardness may be lost. When the indents reached 0.5 mm into the samples the spacing increased to 0.5 mm between every indent until reaching 2.5 mm deep. See Figure 3.6b for the placement of the indents.

For the Knoop measurements the process is very similar to the Vickers. The difference being that the Knoop indent is about 2.8 times longer/wider and shallower than a Vickers indent at the same force applied. Therefore the offset between the indents could be close together depth wise, hence the hardness of the outermost surface could be measured. Knoop was exclusively performed towards the top (mount surface).

3.6 Scanning Electron Microscope

The Scanning Electron Microscope (SEM) was used to get higher resolution pictures of the mounted samples, possibly seeing microstructure hints and get an idea of the composition in the samples with Energy Dispersive X-ray Spectrometry (EDX).

4
Results & Discussion

In this chapter all relevant results will be presented from the residual stress experiments, hardness test and the microstructure of the samples. Discussion of relevant points will be done here as well.

4.1 Physical examination

In this section the results from the examination of the yokes will be presented.

Chemical analysis

The results from the chemical analysis of the off-cut from Sample #1 is present in Table 4.1.

Table 4.1: Chemical content in Sample #1, wt%.

Material	C	Si	Mn	P	S	Cr	Ni	Mo	N
42CrMo4	0.37	0.27	0.70	0.011	0.006	1.11	0.08	0.25	0.014

Compared to the chemical composition in conventional 42CrMo4 steel, see Table 4.2. There are not any large differences towards the powder's chemical composition. C content is a bit too low, as well as S content. What should not be in the composition are Ni and N. The presence of Ni and N could be from cross-contamination of 316L powder since different powders are continually used and changed in the printer, or possibly from the atmosphere regarding N.

Table 4.2: Chemical content in conventional manufactured steel, wt%. Numbers from [23]

Variant		C %	Si %	Mn %	P %	S %	Cr %	Ni %	Mo %
42CrMo4 M (6082),	Min	0.38	0.15	0.60	-	0.020	0.90	-	0.15
MoC 410 M	Max	0.45	0.40	0.90	0.025	0.035	1.20	-	0.30

Surface roughness

The results from the surface roughness measurements are presented in Table 4.3.

Table 4.3: Results from surface roughness measurements, on a as-printed sample, performed top to bottom on the side of the sample perpendicular the build direction.

Sweep	1	2	3	4	5	6	Mean
R_a [µm]	7.79	5.18	6.11	6.92	8.04	7.25	6.88
R_z [µm]	37.68	27.44	31.95	36.19	40.48	37.07	35.10

4.2 Residual stresses

Result within this section is from the measurements performed with XRD

Surface stresses

From the surface measurements performed on all samples, the results are presented in Figure 4.1 for the mount surface of the yokes. That is the top part of the sample, the last bit that is printed. For the surface stress measurements in the build direction, the results are visible in Figure 4.2.

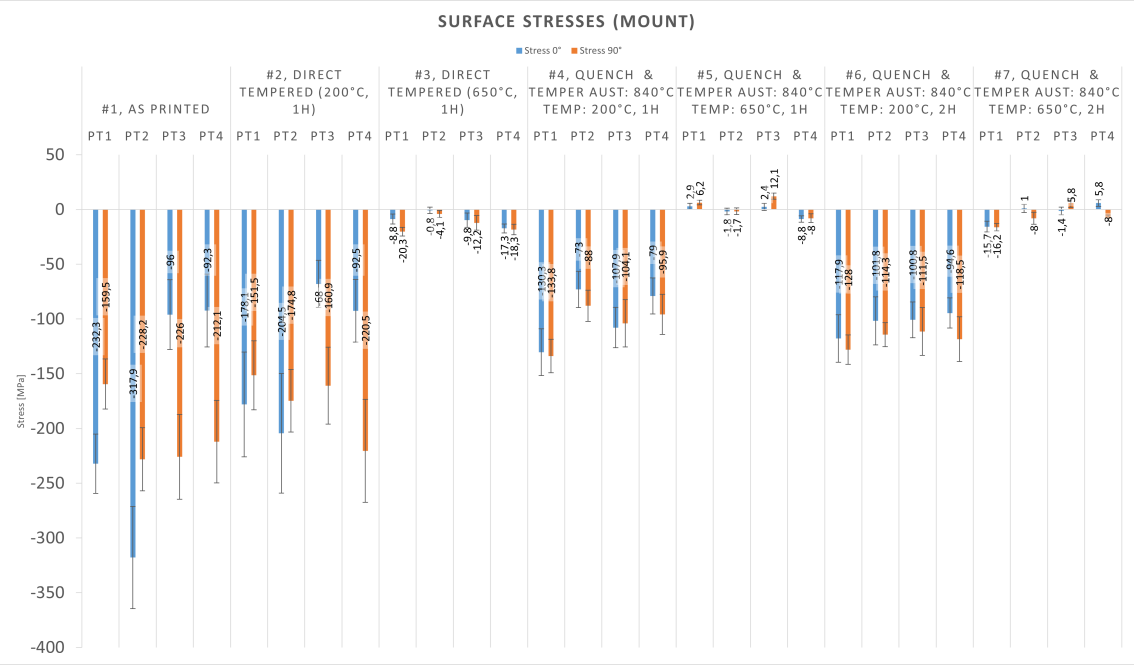

Figure 4.1: Diagram of the results from the surface measurements on the mount surface of the yokes, an enlarged table is visible in Appendix B.1

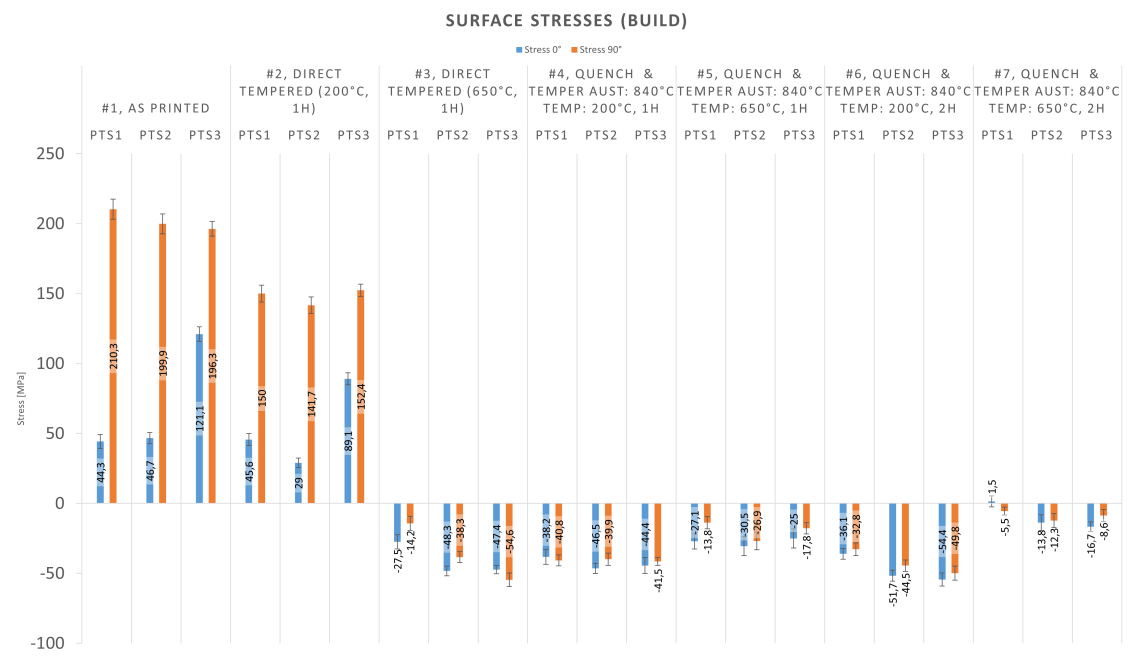

Figure 4.2: Diagram of the results from the surface measurements on the mount surface of the yokes, an enlarged table is visible in Appendix C.1

As seen in Figure 4.1 and 4.2, there is large amounts of tensile stresses in the As-printed sample in the build direction and large compressive stresses on the mount (top) surface. The trend is still visible on Sample #2, direct tempered at 200°C for one hour, no direct visible or notable change in stresses between these samples. The compressive stresses present on the mount surface is rather expected due to the fast cooling the melt is exposed to, leaving an untempered martensitic structure at the top. Since the top layers is not exposed to the re-heating and re-melting the previous layers further down the build structure, resulting in a tempered martensitic structure, further discussion in section 4.3. Sample #3 express a notable decrease in both compressive and tensile stresses, there the tensile stresses are almost gone from the sample. The compressive stresses on the mount surface is still there but to a much lower extent.

Sample #4–#7, the samples being austenitized, express vastly different characteristics. There are high compressive stresses, especially in Sample #4 and a bit lower in Sample #6. No notable stresses are registered in Samples #5 and #7, there are some stresses registered but they are so small that the samples can be considered stress free.

The results from the heat treatment of the pieces that have been austenized, quenched and tempered are rather expected, the samples respond well to the heat cycles. There Sample #4 exhibits excellent properties with compressive stresses in both build direction and on the mount surface, ideal for applications where fatigue is a factor. In this case for injector yokes the cyclic forces are so small that they are negligible. The interesting results are from Sample #3, the Direct Tempered

at 650°C. It is nearly stress free on the mount surface and exhibits compressive stresses in the build direction. It could be because inaccurate measurements due to the surface roughness from the printing, since no contouring was applied during printing and the measurement depth of the equipment reaches 10µm deep. Effectively only measuring the peaks of the surface, see Figure 4.3

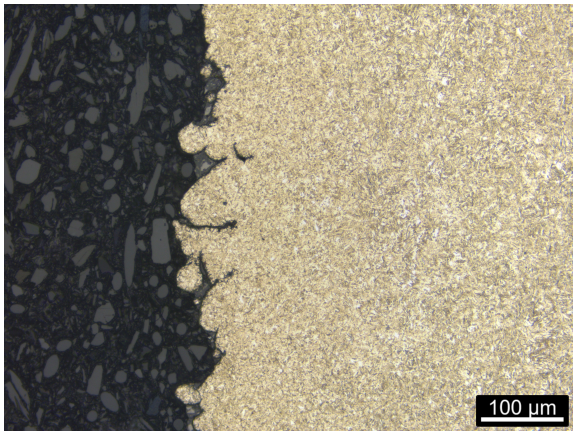

Figure 4.3: Irregular surface that could cause inaccurate residual stress measurements, mounted sample M4#2 at 200x magnification

The most interesting results are from Sample #1 and #2, that have high tensile stresses in the build direction. Considering the previous statement that surface-roughness is a source of inaccurate measurements, the readings from the measurements are so large that it is unlikely to be an inaccurate reading on two different samples. This could be one of several explanations why low-alloy steels have been hard to print successfully without cold cracking [4].

Depth profile

From the results of the surface measurements, a depth profile was the natural continuation in order to examine the stress-evolution further. This is especially interesting to understand for Sample #1 and #2, where large tensile stresses were seen on the surface. The depth profile was done on the side (point PTS2) of the yokes, see results in Figure 4.4–4.7b. Considering the previous statement that surface roughness is a source of inaccurate measurements, the readings from the measurements are so large that it is unlikely to be an inaccurate reading on two different samples.

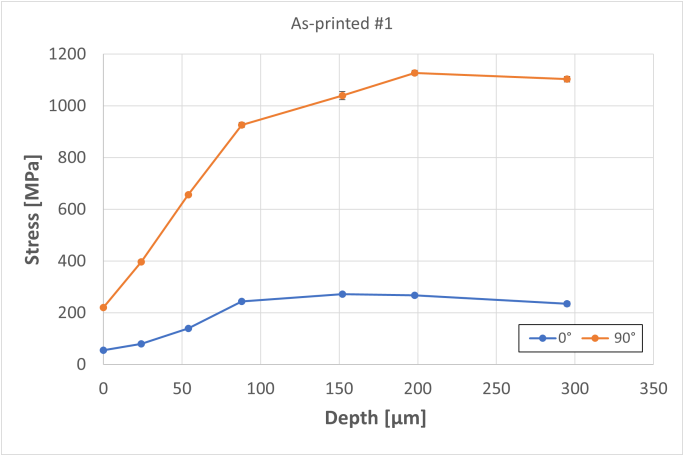

Figure 4.4: Depth profile results from Sample #1

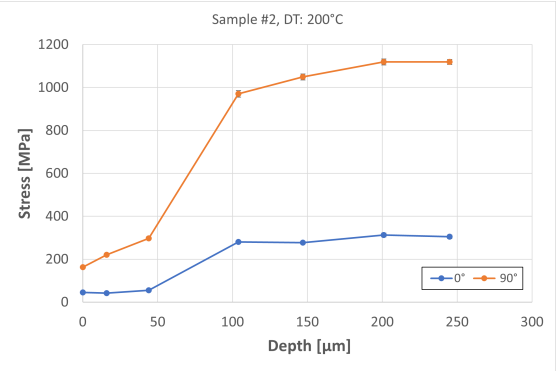

(a) Sample #2

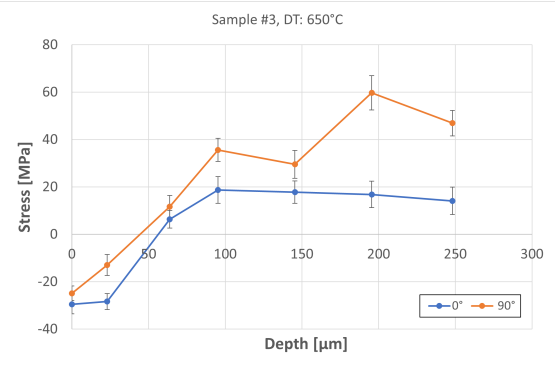

(b) Sample #3

Figure 4.5: Depth profile results from Sample #2 and #3

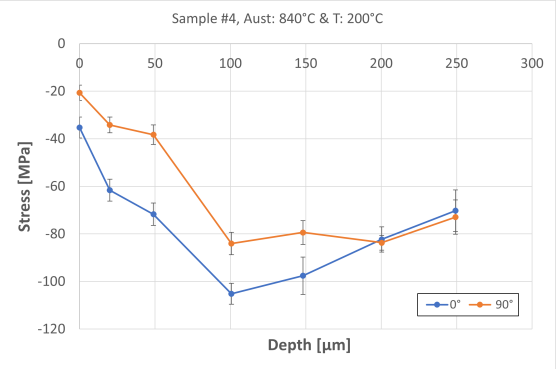

(a) Sample #4

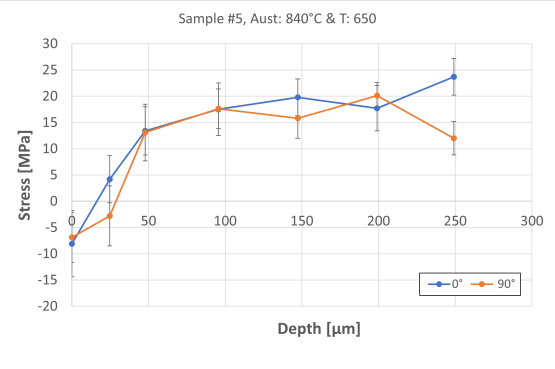

(b) Sample #5

Figure 4.6: Depth profile results from Sample #4 and #5

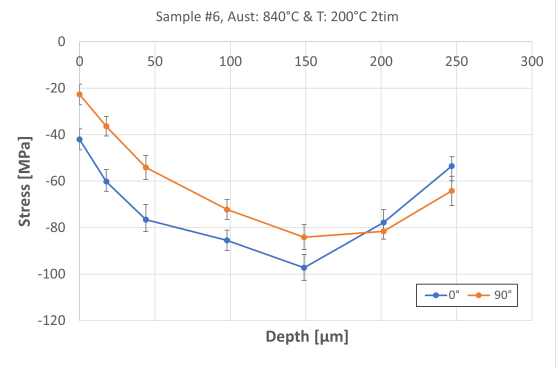

(a) Sample #6

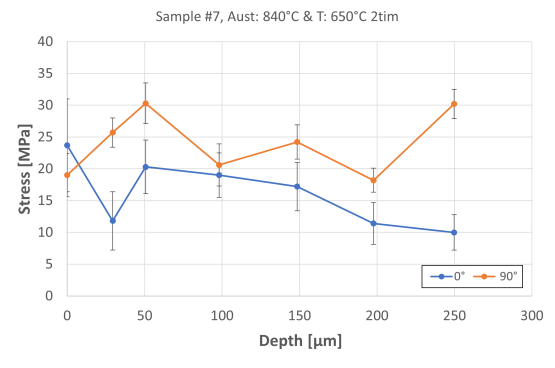

(b) Sample #7

Figure 4.7: Depth profile results from Sample #6 and #7

The results from the depth profiles reveal some surprises, especially when analysing Samples #1 and #2 with enormous tensile stresses that reach up towards 1.1 GPa in the near-surface of the material. These are stresses at, or in, the vicinity of the

yield stress for 42CrMo4. Steel manufacturer Ovako states that the yield stress for conventionally manufactured 42CrMo4 is around 1.0–1.2 GPa [23]. The noteworthy results are that the high tensile stresses are not towards the surface of the samples, but rather more towards the bulk of the material.

It is believed that it could have something to do with the additive process itself. Since no contouring have been done during the printing the surface is rough, with a mean R_z value of ∼35 µm across all sweeps, see Table 4.3. With the surface being this rough, the hypothesis is that the powder has sintered/partially melted to the surface and has no stresses. Hence it contributes to the low residual stress measurements on the surface. With the XRD only being able to measure no deeper than ∼10 µm, the stresses in the depth profile will be lower near the surface. When approaching a depth of ∼50 µm there are more material around to resist movement and thus increasing residual stresses. A contouring pass around the edge perimeter with the laser could be used to reduce the surface roughness and also possibly reduce the residual stress by not fully remelt the solidified metal. However, this is only an hypothesis and will need much more extensive research to reach any conclusion regarding the residual stresses.

4.3 Microstructure

The analysis of the microstructure in OM of all the samples, it revealed a microstructure consisting of tempered- and un-tempered martensite. The untempered martensite was visible on the top surface on Sample #1 (As-printed) and #2 (Direct Temper 200°C), see Figure 4.10a and 4.10b, otherwise it was a relatively homogeneous microstructure of tempered martensite with some difference of fine and coarse martensite between the samples from different heat treatments.

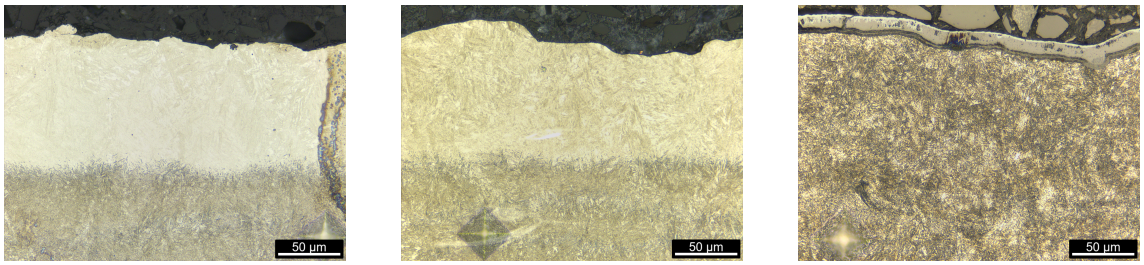

(a) Sample#1, As-printed, microstructure of the top untempered layer

(b) Sample#2, DT 200°C, microstructure of the top untempered layer

(c) Sample#3, DT 650°C, microstructure of the top layer

Figure 4.8: Microstructures of Sample #1, #2 and #3, with a Vickers indent at 150 µm depth from the surface.

In Hearn et.al [41], the reasoning for phenomenon of the untempered martensite in the outer most top layer is explained. To form a martensitic structure the steel needs to be cooled fast, and during printing with LB-PBF the cooling rate of the melt pool goes up towards rates of 10^6 K/s [42]. With such a fast cooling rate the carbon atoms are not given any time to diffuse, and thus create a martensitic structure.

The reason for only the top layers to exhibit such a microstructure is due to the lack of intrinsic heat treatment, these outer most layers have not been subjected to the same kind of in-situ tempering as the rest of the layers. During the printing operation the laser beam typically has a melt pool 100 µm, and with the powder layer varying around 20–80 µm thick, the re-melting of previous layers can be up to 4-5 powder-layers [4].

The microstructure on the top most layer are also visibly more coarse than the tempered martensitic structure ∼100 µm from the top layer. The same microstructure is only slightly visible in Sample #3, since the temper temperature is at the starting area to recrystallize [6], but not sufficient time enough to fully recrystallise the material to a homogeneous structure. There is also a visible oxide layer on Sample #3, this is due to not using any protective gas used during the tempering (as the heat treatment was developed to be able to be used with conventional manufactured steel and not tailored towards AM).

For Sample #4–#7 the microstructure is thoroughly homogeneous, showing lath martensite, as to be expected from a conventionally manufactured 42CrMo4 steel, there were not any real surprises. The untempered martensitic layer at the top of the printed parts are not visible, as to be expected when austenize at 840°C.

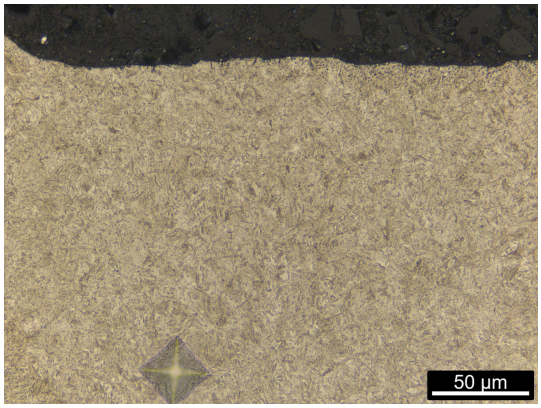

(a) Sample#4 through-hole (M4#1), Q&T 200°C 1h, microstructure of the top layer

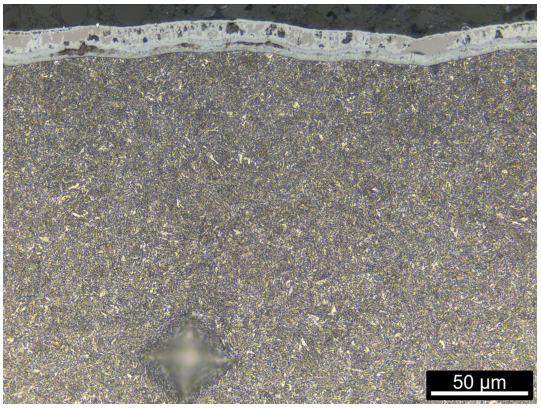

(b) Sample#5 through-hole (M5#1), Q&T 650°C 1h, microstructure of the top layer

Figure 4.9: Microstructures of Sample #4 and #5, with Vickers indent at 150 µm depth.

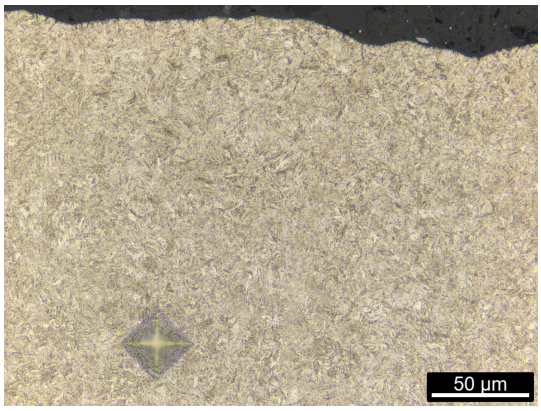

(a) Sample#6 through-hole (M6#1), Q&T 200°C 2h, microstructure of the top layer

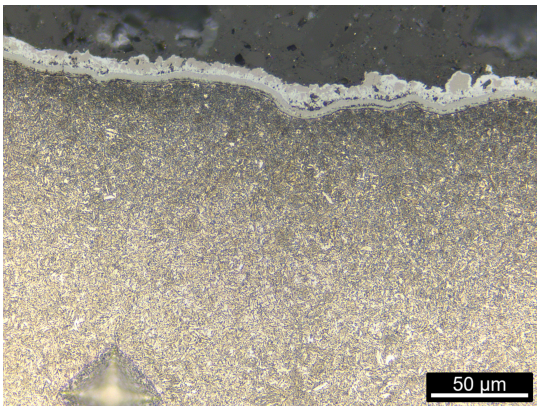

(b) Sample#7 through-hole (M7#1), Q&T 650°C 2h, microstructure of the top layer

Figure 4.10: Microstructures of Sample #6 and #7, with Vickers indent at 150 µm depth.

There were some porosity found in all samples, some in bulk material and some close to the surfaces, both gas-porosity and lack-of-fusions. In one mounted sample, M2#2, cracks were discovered. Three cracks at different build levels, that seemed to start at the surface. However, this is only speculative and not confirmed. The cracks were only found in this one sample across 14 mounted samples, which is not seen as a pattern. With the results from the residual stress depth profile, the conclusion that the cracks developed due to the stresses seem reasonable. One of the three cracks, see Figure 4.11, was about 5 mm deep.

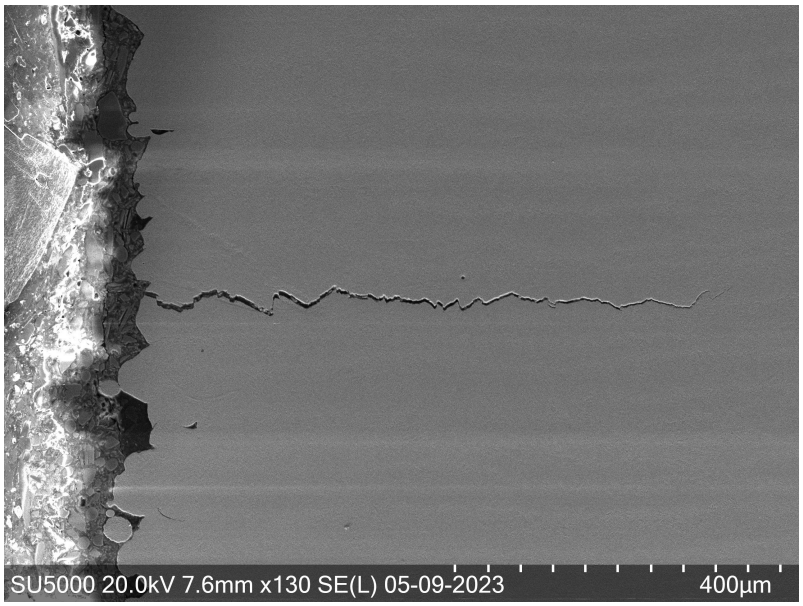

Figure 4.11: The large crack discovered in the fork of Sample#2 (M2#2), using SEM

4.4 Hardness measurement

The overall hardness values were in line with the expected values from heat treated 42CrMo4. Most notably is Sample #1, #2 and #3, Figure 4.12, 4.13a and 4.13b, that exhibits notably different hardness values depending on the where the profiles were retrieved from the sample. This behaviour can be explained due to in-situ macro tempering from the printing process itself [43]. With the build plate heated constantly to 180°C, and the core of the parts retaining heat, the parts will self temper to some degree. The trend is especially noticeable when comparing the profile of the "Top" and "Bottom" profiles. At 0.5–1mm into the part, the profiles conjugate and reach a similar hardness value. For sample #4–#7, they exhibit a pattern very similar to conventionally manufactured 42CrMo4 that has been heat-treated at the same temperatures. Sample #1 and #2 exhibit a hardness value 50–100HV higher than conventional rolled bar stock [23].

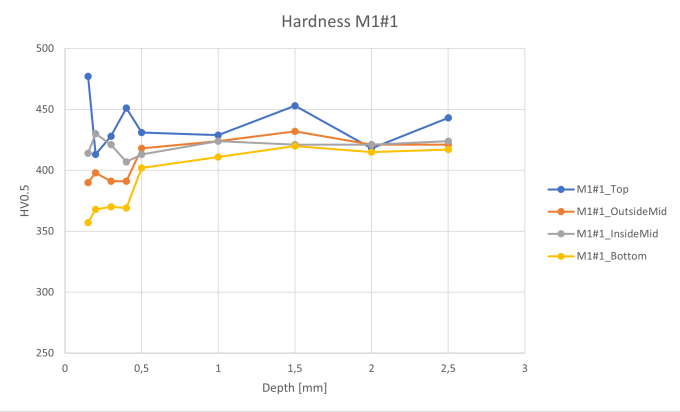

Figure 4.12: Hardness profiles from the through-hole in Sample#1 (M1#1), As-printed, the profiles are taken from each of the four surfaces. Top (mount), Inside and outside of the through hole and the bottom (print start).

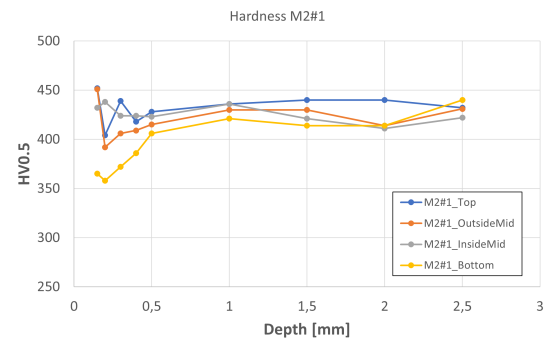

(a) Sample #2, through-hole (M2#1), DT 200°C

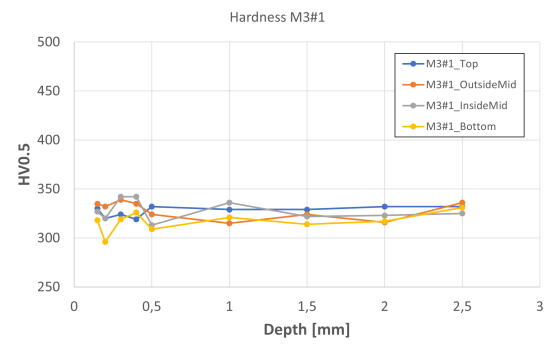

(b) Sample #3, through-hole (M3#1), DT 650°C

Figure 4.13: Hardness profiles for M2#1 and M3#1, the profiles are taken from each of the four surfaces. Top (mount), Inside and outside of the through hole and the bottom (print start).

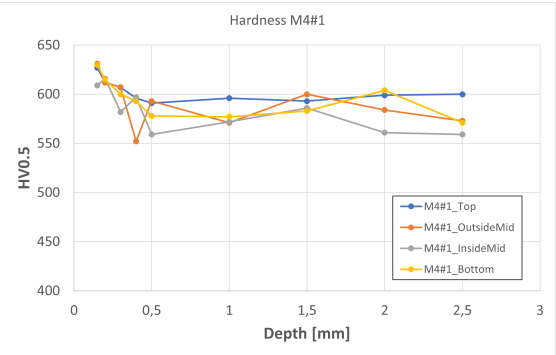

(a) Sample #4, through-hole (M4#1), Q&T 200°C 1h

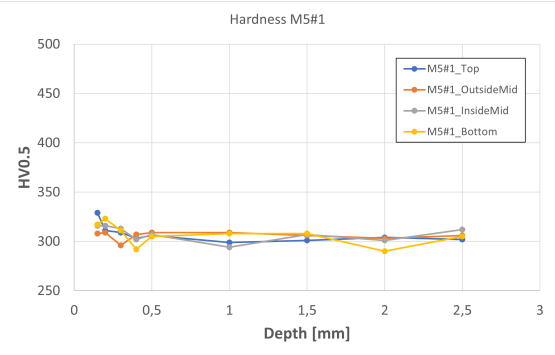

(b) Sample #5, through-hole (M5#1), Q&T 650°C 1h

Figure 4.14: Hardness profiles for M4#1 and M5#1, the profiles are taken from each of the four surfaces. Top (mount), Inside and Outside of the through hole and the bottom (print start).

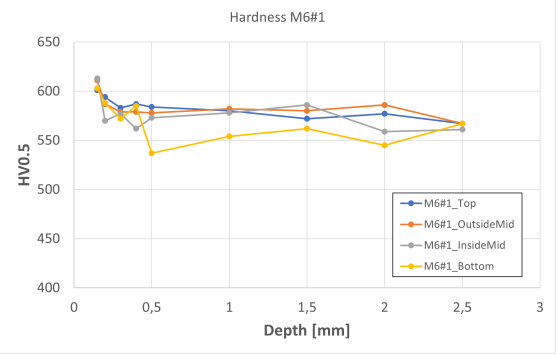

(a) Sample #6, through-hole (M6#1), Q&T 200°C 2h

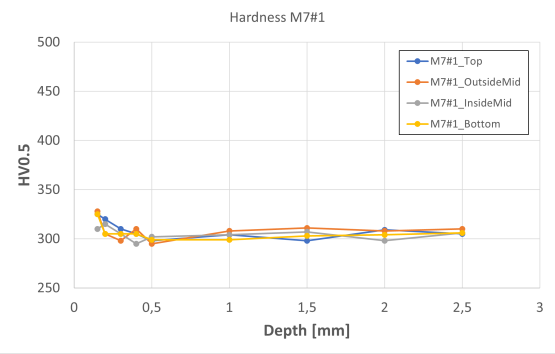

(b) Sample #7, through-hole (M7#1), Q&T 650°C 2h

Figure 4.15: Hardness profiles for M6#1 and M7#1, the profiles are taken from each of the four surfaces. Top (mount), Inside and outside of the through hole and the bottom (print start).

From the profiles could not any indications towards the high residual stresses present in Sample #1 and #2 be seen. Therefore, some extra profiles were taken on the side of Samples #1 and #2 with 0.2kg of force to possibly see any shift in hardness, see Table 4.4.

From the Knoop hardness measurements, there is a trend of a hardness peak at 120 µm, compared to the residual stress depth profiles that indicates a peak in residual stresses at a depth of 200 µm. The series is too small to draw any conclusions regarding hardness compared to residual stresses, and further hardness profiles has to be taken to be able to draw any conclusions.

Table 4.4: Hardness profile of the outer edge on Sample #1 and #2

Specimen	Depth [mm]	Hardness HV0.2	Diagonal [µm]
M1#1 Outside	0,09	423	29,62
	0,12	523	26,639
	0,15	454	28,583
	0,2	436	29,167
M2#1 Outside	0,09	401	30,398
	0,12	480	27,806
	0,15	403	30,334
	0,2	400	30,463

Knoop

The hardness profiles were taken before the etching and the examination of the microstructure. When analysing the etched samples there was a clear difference in microstructure between the top layers compared to the bulk of the material. The untempered martensite in the top layer had a much coarser microstructure than the tempered martensite on the bulk. Due to the recommended placement distance, the Vickers indents were placed too far from the edge to be able to measure the untempered layer 150 µm deep. Therefore, Knoop profiles were taken as well, targeted at the outer most top layer, see Figures 4.16b–4.19b. Knoop is a somewhat different scale that Vickers, and confirming that via tables from steel manufacturers [44] and own test, see Figure 4.16a, they differ approximate ∼30 units.

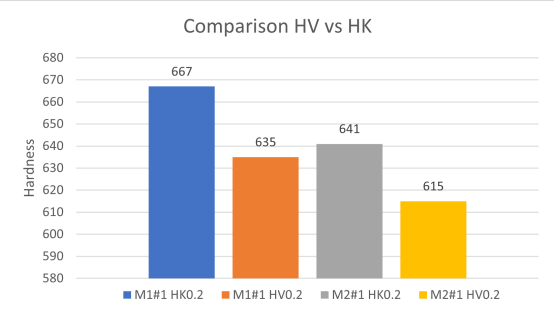

(a) Comparison between HV0.2 and HK0.2 to see a rough difference between the two, and to get an idea of how the results compare to the hardness profiles taken with HV0.2.

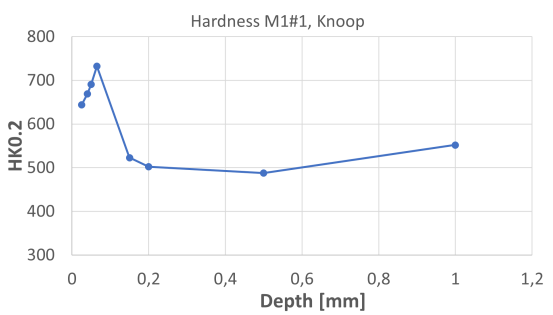

(b) Knoop profile for Sample#1, through-hole (M1#1), measured from the top of the mount surface.

Figure 4.16: Comparison between HV and HK, a) and Knoop hardness profile for M1#1, b). The profile is taken from the top (mount).

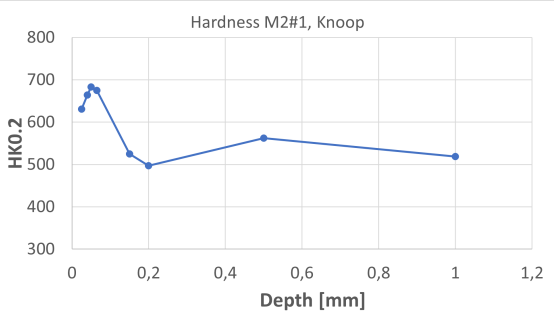

(a) Knoop profile for Sample#2, through-hole (M2#1), measured from the top of the mount surface

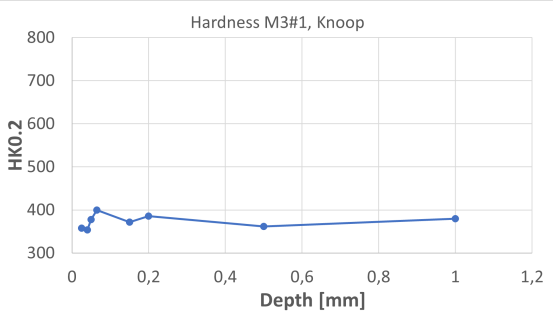

(b) Knoop profile for Sample#3, through-hole (M3#1), measured from the top of the mount surface

Figure 4.17: Knoop hardness profiles for M2#1 and M3#1, the profiles are taken from the top (mount).

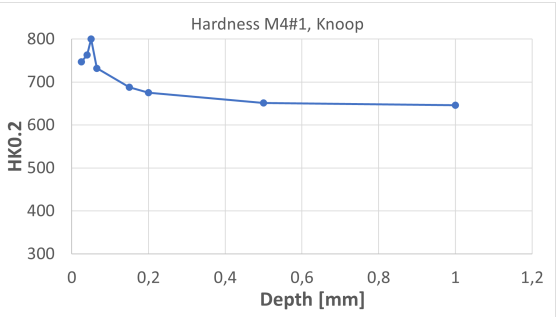

(a) Knoop profile for Sample#4, through-hole (M4#1), measured from the top of the mount surface

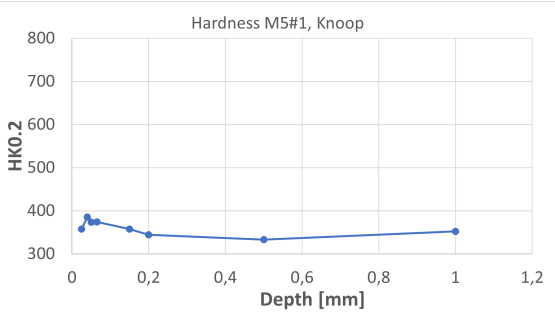

(b) Knoop profile for Sample#5, through-hole (M5#1), measured from the top of the mount surface

Figure 4.18: Knoop hardness profiles for M4#1 and M5#1, the profiles are taken from the top (mount).

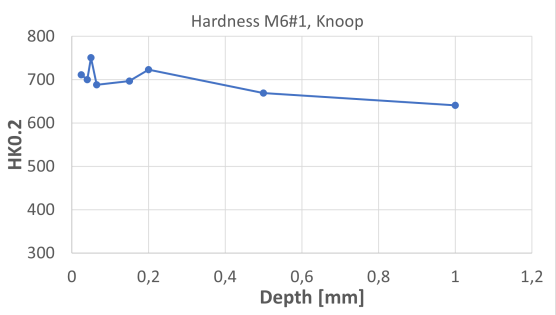

(a) Knoop profile for Sample#6, through-hole (M6#1), measured from the top of the mount surface

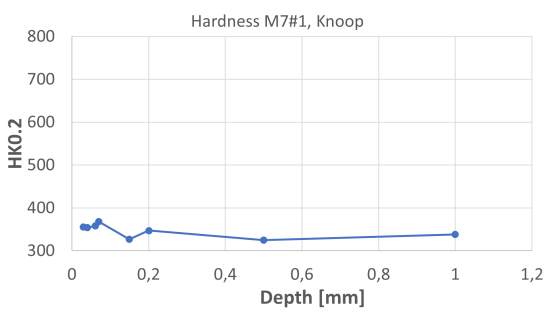

(b) Knoop profile for Sample#7, through-hole (M7#1), measured from the top of the mount surface

Figure 4.19: Knoop hardness profiles for M6#1 and M7#1, the profiles are taken from the top (mount).

A trend visible on almost every sample is the increasing hardness in the top layer until reaching a depth of ∼0.1mm, which is the edge of the tempered martensite that exhibit a transition of quite coarse and fine martensite on Sample #1 and #2. This transition is not visible on any other sample, rather they exhibit a homogeneous tempered martensitic microstructure through the whole sample. This could indicate that it can be related to the columnar grain structure present in parts manufactured with LB-PBF [45]. To further understand this, more research using EBSD is needed.

5
Summary

In this project the effect of heat treatment on residual stresses was examined and analysed, these are the conclusions that can be drawn:

5.1 Conclusions

- The response of the heat treatment goes in line with how conventional manufactured 42CrMo4 behaves during heat treatment.
- The residual stresses reaches a peak of around 1100 MPa 150μm deep in a as-printed and direct tempered at 200°C sample. However, more research and experiments is needed to fully confirm this.

  The sample direct tempered at 650°C exhibits good and possibly usable properties where the compressive residual stresses is still left at the surface, and the tensile stresses is considerable lower than in the as-printed and DT 200°C state. Direct temper could be an option at elevated tempering temperatures. To minimise the oxide scales that develop during tempering, a protective gas applied during tempering would be beneficial.
- The surface hardness is high on the as-printed and the direct tempered at 200°C samples, and is slightly lower in the tempered sample. That could be remedied with a longer temper period and more research. More experiments and research is needed. The rest of the heat treatments exhibits comparable hardness to conventional 42CrMo4 that have been heat treated in similar heat treatments [23].

5.2 Future work

The results from the project exposed a number of question and uncertainties, especially the source of the residual stresses. The recommended future work would be:

- Add a contouring pass during printing, to see if the residual stress behaviour differ from the stresses seen on the parts analysed in this project.
- A residual stress analysis deeper into the material would be interesting, not only a even more thorough analysis but deeper into the bulk as well.
- An microstructure analysis using EBSD would be interesting as well to see how the columnar grains behave when subjected to different heat treatments. Also if there is any influence on residual stress due to the grain structure.

- Explore more heat treatments such as; nitriding, gas carburizing and induction hardening, as well as different tempering temperatures for both Q&T and DT.
- Mechanical testing, tensile and fatigue testing on heat treated samples
- Explore other post-processes such as; Shot peening and testing how it influences the residual stresses, both for as-printed as well as heat treated samples.

Bibliography

[1] H.M. Khan et al. "Influence of the post-processing operations on surface integrity of metal components produced by laser powder bed fusion additive manufacturing: a review". In: *Machining Science and Technology* 25.1 (2021), pp. 118–176. DOI: 10.1080/10910344.2020.1855649. eprint: https://doi.org/10.1080/10910344.2020.1855649. URL: https://doi.org/10.1080/10910344.2020.1855649.

[2] V. Petrovic et al. "Additive manufacturing solutions for improved medical implants". In: *Biomedicine* 2012 (2012), pp. 147–180.

[3] U.M. Dilberoglu et al. "The Role of Additive Manufacturing in the Era of Industry 4.0". In: *Procedia Manufacturing* 11 (2017). 27th International Conference on Flexible Automation and Intelligent Manufacturing, FAIM2017, 27-30 June 2017, Modena, Italy, pp. 545–554. ISSN: 2351-9789. DOI: https://doi.org/10.1016/j.promfg.2017.07.148. URL: https://www.sciencedirect.com/science/article/pii/S2351978917303529.

[4] W. Hearn. "Development of Structural Steels for Powder Bed Fusion - Laser Beam". PhD thesis. Chalmers University of Technology, 2023. ISBN: 978-91-7905-778-7.

[5] E.F. Wente, E.F. Wondris, and J. Nutting. "steel". In: *Encyclopedia Britannica*. 2022.

[6] T. Holm, P. Olsson, and E. Troell. *Steel and Its Heat Treatment: A Handbook*. IVF research publication: Institutet för Verkstadsteknisk Forskning. SWEREA IVF, 2012. ISBN: 978-91-86401-11-5.

[7] ASM Handbook Committee. *ASM Handbook. Vol 1. Properties and Selection: Irons, Steels, and High-Performance Alloys*. Vol. 1. ASM International, 1990, pp. 140–194. ISBN: 978-1-62708-161-0.

[8] ASM Handbook Committee. *ASM Handbook: Steel Heat Treating Technologies*. Vol. 4B. ASM International, 2014. ISBN: 978-1-62708-166-5.

[9] ASM Handbook Committee. *ASM Handbook. Vol 1. Properties and Selection: Irons, Steels, and High-Performance Alloys*. Vol. 1. ASM International, 1990, pp. 451–463. ISBN: 978-1-62708-161-0.

[10] P.B. Srinivasanand, C.V. Krishnakumar, and N. Krishnaraj. "Sliding wear behavior of salt bath nitrocarburized medium carbon steel". In: *J. Mater. Eng. Perform.* 11.5 (Oct. 2002), pp. 509–515.

[11] R. Yamanoglu et al. "Sintering and microstructure characteristics of 42CrMo4 steel processed by spark plasma sintering". In: *Metals and Materials International* 19 (2013), pp. 1029–1034.

[12] C. Li, Y. Wang, and B. Han. "Microstructure, hardness and stress in melted zone of 42CrMo steel by wide-band laser surface melting". In: *Optics and Lasers in Engineering* 49.4 (2011), pp. 530–535.

[13] D. Chaouch, S. Guessasma, and A. Sadok. "Finite Element simulation coupled to optimisation stochastic process to assess the effect of heat treatment on the mechanical properties of 42CrMo4 steel". In: *Materials & Design* 34 (2012), pp. 679–684.

[14] ASM Handbook Committee. *Alloying: Understanding the basics, 3rd Edition*. ASM International, Apr. 2005. ISBN: 978-0-87170-744-4.

[15] H. Karlsson. *Role of Surface Oxides in Sintering of Chromium-alloyed Steel Powder*. 2005.

[16] I. Olefjord. "Temper embrittlement". In: *International Metals Reviews* 23.1 (1978), pp. 149–163. DOI: 10.1179/imtr.1978.23.1.149. URL: https://doi.org/10.1179/imtr.1978.23.1.149.

[17] S. Sanchez et al. "Powder Bed Fusion of nickel-based superalloys: A review". In: *International Journal of Machine Tools and Manufacture* 165 (2021), p. 103729. ISSN: 0890-6955. DOI: https://doi.org/10.1016/j.ijmachtools.2021.103729. URL: https://www.sciencedirect.com/science/article/pii/S0890695521000390.

[18] J. Wegner et al. "Influence of process gas during powder bed fusion with laser beam of Zr-based bulk metallic glasses". In: *Procedia CIRP* 94 (2020). 11th CIRP Conference on Photonic Technologies [LANE 2020], pp. 205–210. ISSN: 2212-8271. DOI: https://doi.org/10.1016/j.procir.2020.09.039. URL: https://www.sciencedirect.com/science/article/pii/S2212827120312245.

[19] A.B. Badiru, V.V. Valencia, and D. Liu. *Additive Manufacture Handbook: Product Development for the Defence Industry*. Taylor & Francis Group, 2017. ISBN: 978-1-4822-6408-12.

[20] Chao Cai and Kun Zhou. "Chapter 7 - Metal additive manufacturing". In: *Digital Manufacturing*. Ed. by C.D. Patel and C-H. Chen. Elsevier, 2022, pp. 247–298. ISBN: 978-0-323-95062-6. DOI: https://doi.org/10.1016/B978-0-323-95062-6.00005-X. URL: https://www.sciencedirect.com/science/article/pii/B978032395062600005X.

[21] J. Wadsworth and O.D. Sherby. "On the Bulat—Damascus steels revisited". In: *Progress in Materials Science* 25.1 (1980), pp. 35–68. ISSN: 0079-6425. DOI: https://doi.org/10.1016/0079-6425(80)90014-6. URL: https://www.sciencedirect.com/science/article/pii/0079642580900146.

[22] K-E. Thelning. *Bofors Handbok: Värmebehandling av Stål*. Maskinaktiebolaget Karlebo, 1967.

[23] Ovako. *Material data sheet, Steel grade 42CrMo4*. 2023. URL: https://steelnavigator.ovako.com/steel-grades/42crmo4/ (visited on 02/28/2023).

[24] G. R. Speich and W. C. Leslie. *Tempering of Steel*. 1972.

[25] Jamison L. Bartlett and Xiaodong Li. "An overview of residual stresses in metal powder bed fusion". In: *Additive Manufacturing* 27 (2019), pp. 131–149. ISSN: 2214-8604. DOI: https://doi.org/10.1016/j.addma.2019.02.

020. URL: https://www.sciencedirect.com/science/article/pii/S221486041930051X.

[26] P J Withers. "Residual stress and its role in failure". In: *Reports on Progress in Physics* 70.12 (Nov. 2007), p. 2211. DOI: 10.1088/0034-4885/70/12/R04. URL: https://dx.doi.org/10.1088/0034-4885/70/12/R04.

[27] W. Zhang, M. Tong, and N.M. Harrison. "Scanning strategies effect on temperature, residual stress and deformation by multi-laser beam powder bed fusion manufacturing". In: *Additive Manufacturing* 36 (2020), p. 101507. ISSN: 2214-8604. DOI: https://doi.org/10.1016/j.addma.2020.101507. URL: https://www.sciencedirect.com/science/article/pii/S2214860420308794.

[28] ASM Handbook Committee. *ASM Handbook. Materials Characterization (2019 Edition)*. Vol. 10. ASM International, 2019. ISBN: 978-1-62708-211-2.

[29] G.S. Schajer. "Advances in hole-drilling residual stress measurements". In: *Experimental Mechanics* 50.2 (Feb. 2010), pp. 159–168.

[30] W.H. Bragg and W.L. Bragg. "The reflection of X-rays by crystals". In: *Proceedings of the Royal Society of London* 88.605 (1913), pp. 428–438. DOI: https://doi.org/10.1098/rspa.1913.0040.

[31] P.S. Prevey et al. "X-ray diffraction residual stress techniques". In: *ASM International, ASM Handbook.* 10 (1986), pp. 380–392.

[32] L.R.B. Elton and D.F. Jackson. "X-ray Diffraction and the Bragg Law". In: *American Journal of Physics* 34 (1966), pp. 1036–1038. DOI: 10.1119/1.1972439.

[33] T. Fry. "Residual Stress Measurement: XRD Depth Profiling Using Successive Material Removal". In: (2005). ISSN: 1744-3911.

[34] ASM Handbook Committee. *Handbook of Residual Stress and Deformation of Steel*. ASM International, 2002. ISBN: 0-87170-729-2.

[35] I. C. Noyan and J. B. Cohen. *Residual stress: measurement by diffraction and interpretation*. Springer, 1987.

[36] ASM Handbook Committee. *ASM Handbook. Vol 9. Metallography and Microstructures*. Vol. 9. ASM International, 2004. ISBN: 978-0-87170-760-2.

[37] D. Adamovic and F. Zivic. "Hardness and Non-Destructive Testing (NDT) of Ceramic Matrix Composites (CMCs)". In: *Encyclopedia of Materials: Composites*. Oxford: Elsevier, 2021, pp. 183–201. ISBN: 978-0-12-819731-8. DOI: https://doi.org/10.1016/B978-0-12-819724-0.00074-4. URL: https://www.sciencedirect.com/science/article/pii/B9780128197240000744.

[38] D. Chicot et al. "Comparison of instrumented Knoop and Vickers hardness measurements on various soft materials and hard ceramics". In: *Journal of the European Ceramic Society* 27.4 (2007), pp. 1905–1911. ISSN: 0955-2219. DOI: https://doi.org/10.1016/j.jeurceramsoc.2006.06.011. URL: https://www.sciencedirect.com/science/article/pii/S0955221906004675.

[39] F. Knoop, C.G. Peters, and W.B. Emerson. "A Sensitive Pyramidal-Diamond Tool for Indentation Measurements". In: *Journal of Research of the National Bureau of Standards* 23.1 (July 1939).

[40] H. Karlsson. *New material in PN 469797 (yoke for nozzle holder) for aftermarket*. Unpublished Internal Document. 2013.

[41] W. Hearn and E. Hryha. “Influence of Carbon on the microstructure of Carbon Steels produced by L-PBF”. In: *European Powder Metallurgy Association (EPMA)* (2022).

[42] U. Scipioni Bertoli et al. “In-situ characterization of laser-powder interaction and cooling rates through high-speed imaging of powder bed fusion additive manufacturing”. In: *Materials & Design* 135 (2017), pp. 385–396. ISSN: 0264-1275. DOI: https://doi.org/10.1016/j.matdes.2017.09.044. URL: https://www.sciencedirect.com/science/article/pii/S0264127517308894.

[43] W. Hearn et al. “In situ tempering of martensite during laser powder bed fusion of Fe-0.45C steel”. In: *Materialia* 23 (2022).

[44] PGI Steel. *Hardness Conversion Chart*. 2023. URL: https://pgisteel.com/hardness-conversion-chart/ (visited on 05/30/2023).

[45] A. Shrivastava, S. Anand Kumar, and S. Rao. “5 - Postprocessing challenges in metal AM: Strategies for achieving homogeneous microstructure in Ni-based superalloys”. In: *Advances in Metal Additive Manufacturing*. Ed. by S. Salunkhe, S.T. Amancio-Filho, and J.P. Davim. Woodhead Publishing Reviews: Mechanical Engineering Series. Woodhead Publishing, 2023, pp. 179–202. ISBN: 978-0-323-91230-3. DOI: https://doi.org/10.1016/B978-0-323-91230-3.00001-9. URL: https://www.sciencedirect.com/science/article/pii/B9780323912303000019.

A

Cooling diagrams for 42CrMo4

A.1 Continious Cooling Transformation

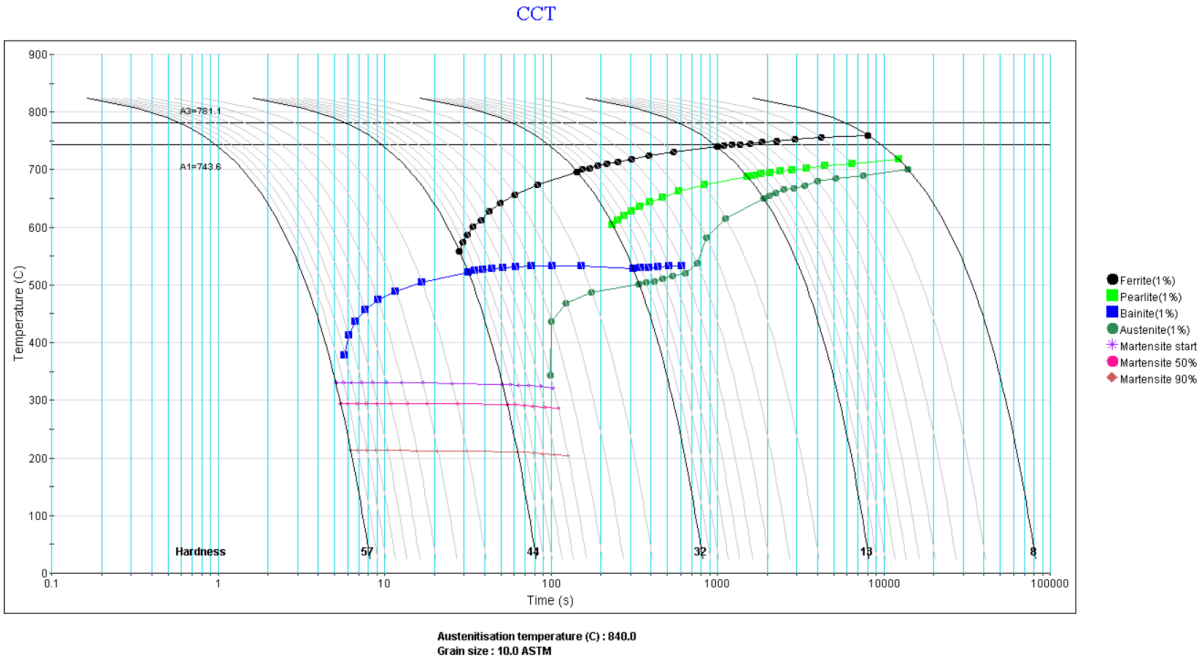

Figure A.1: CCT–diagram for 42CrMo4

A.2 Time-Temperature Transformation

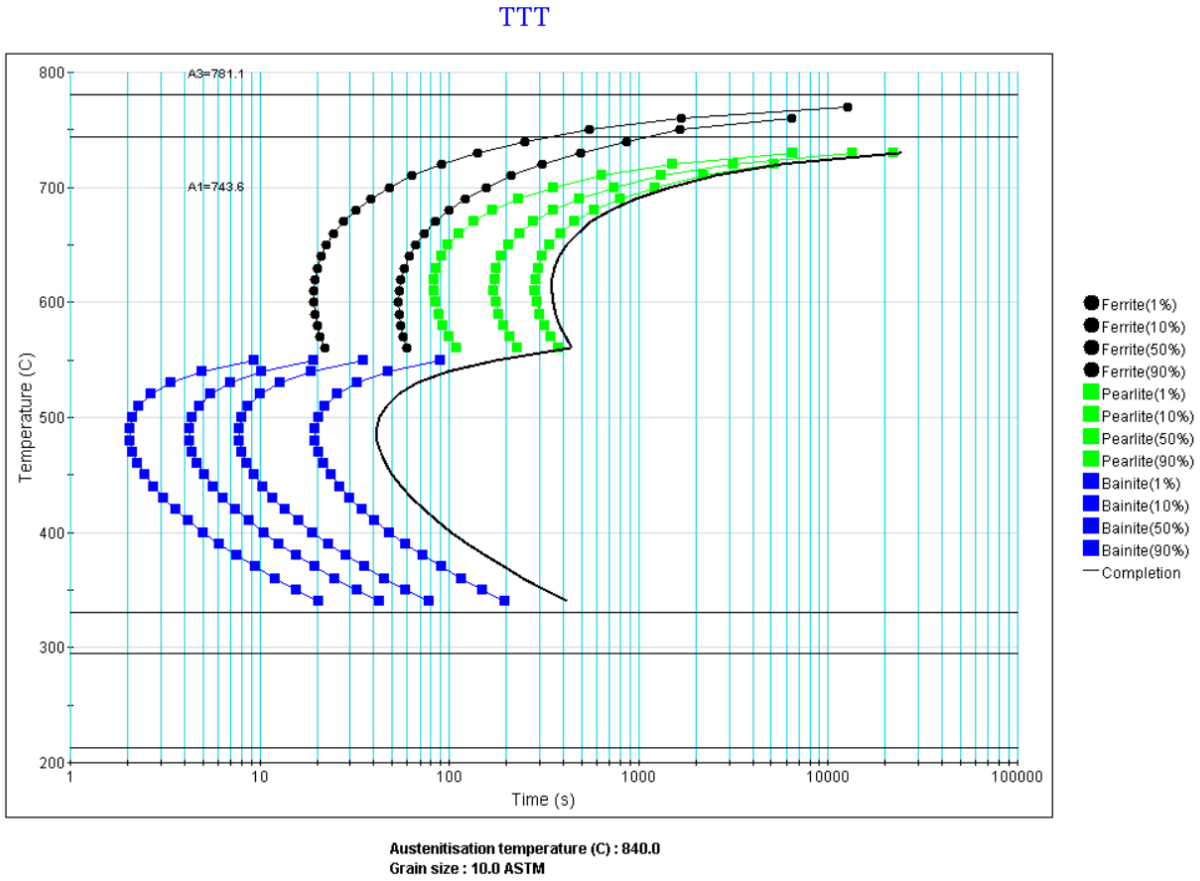

Figure A.2: TTT–diagram for 42CrMo4

B

Residual stress, Mount surface

B.1 Raw numbers

Sample	Measure point	Stress 0° [MPa]	Stress 90° [MPa]	Deviation (+/–)
#1, As Printed	PT1	-232,3	-159,5	27,1
	PT2	-317,9	-228,2	46,6
	PT3	-96	-226	31,9
	PT4	-92,3	-212,1	33,3
#2, Direct tempered (200°C, 1h)	PT1	-178,1	-151,5	47,8
	PT2	-204,5	-174,8	54,6
	PT3	-68	-160,9	21,5
	PT4	-92,5	-220,5	28,6
#3, Direct tempered (650°C, 1h)	PT1	-8,8	-20,3	4,6
	PT2	-0,8	-4,1	3
	PT3	-9,8	-12,2	6,5
	PT4	-17,3	-18,3	4,1
#4, Quench & Temper Aust: 840°C Temp: 200°C, 1h	PT1	-130,3	-133,8	21,4
	PT2	-73	-88	16,6
	PT3	-107,9	-104,1	18,5
	PT4	-79	-95,9	16,5
#5, Quench & Temper Aust: 840°C Temp: 650°C, 1h	PT1	2,9	6,2	2,8
	PT2	-1,8	-1,7	3
	PT3	2,4	12,1	3,3
	PT4	-8,8	-8	2,9
#6, Quench & Temper Aust: 840°C Temp: 200°C, 2h	PT1	-117,9	-128	21,7
	PT2	-101,8	-114,3	22
	PT3	-100,8	-111,5	16,3
	PT4	-94,6	-118,5	13,8
#7, Quench & Temper Aust: 840°C Temp: 650°C, 2h	PT1	-15,7	-16,2	4,9
	PT2	1	-8	3,7
	PT3	-1,4	5,8	3,5
	PT4	5,8	-8	3,1

B.2 Table, Mount surface

Table B.1: Table of the results from the surface measurements on the mount surface of the yoke

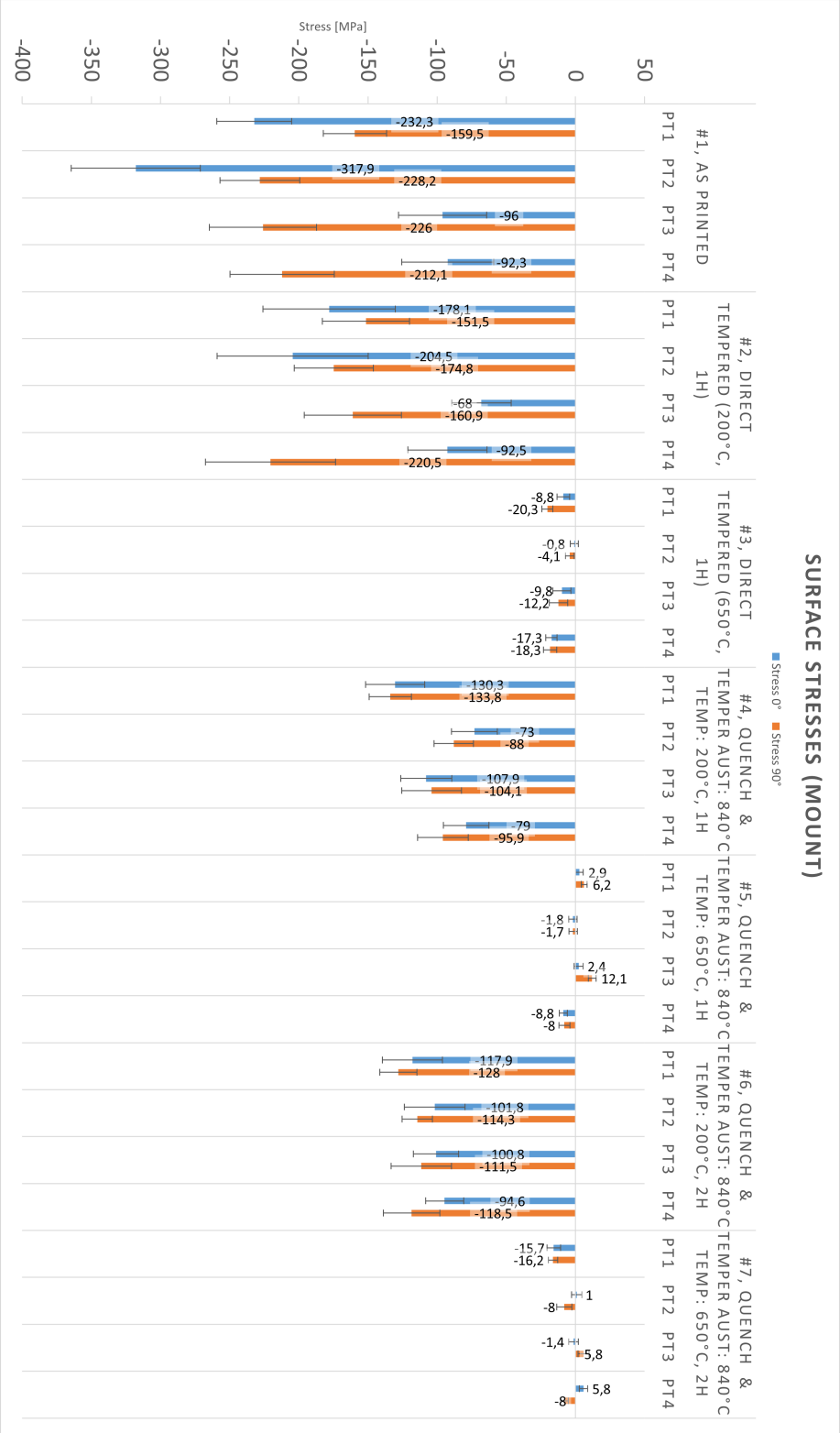

C

Residual stress, Build surface

C.1 Raw numbers

Sample	Measure point	Stress 0° [MPa]	Stress 90° [MPa]	Deviation (+/–)
#1, As Printed	PTS1	44,3	210,3	4,9
	PTS2	46,7	199,9	4
	PTS3	121,1	196,3	5,2
#2, Direct tempered (200°C, 1h)	PTS1	45,6	150	4,3
	PTS2	29	141,7	3,4
	PTS3	89,1	152,4	4,3
#3, Direct tempered (650°C, 1h)	PTS1	-27,5	-14,2	5,1
	PTS2	-48,3	-38,3	3,4
	PTS3	-47,4	-54,6	2,9
#4, Quench & Temper Aust: 840°C & Temp: 200°C, 1h	PTS1	-38,2	-40,8	5,3
	PTS2	-46,5	-39,9	3,7
	PTS3	-44,4	-41,5	5,8
#5, Quench & Temper Aust: 840°C & Temp: 650°C, 1h	PTS1	-27,1	-13,8	5,5
	PTS2	-30,5	-26,9	6,8
	PTS3	-25	-17,8	6,8
#6, Quench & Temper Aust: 840°C & Temp: 200°C, 2h	PTS1	-36,1	-32,8	3,9
	PTS2	-51,7	-44,5	4
	PTS3	-54,4	-49,8	4,7
#7, Quench & Temper Aust: 840°C & Temp: 650°C, 2h	PTS1	1,5	-5,5	3,9
	PTS2	-13,8	-12,3	5,7
	PTS3	-16,7	-8,6	3,4

C.2 Table, Build surface

Table C.1: Table of the results from the surface measurements on the build surface of the yokes

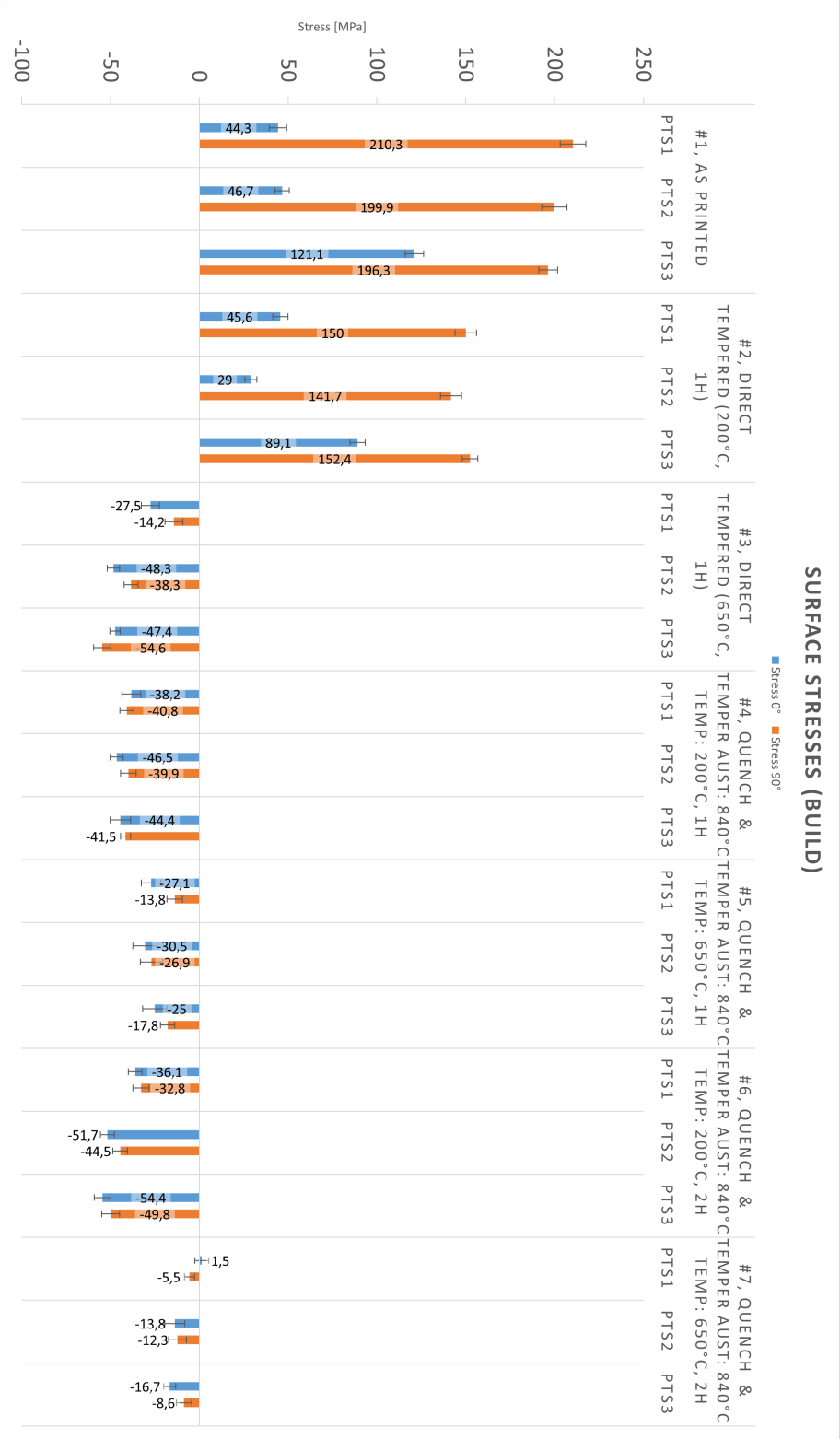

D
Mounted samples, naming

Table D.1: Tabular of the naming for the 14 different mounted samples

Cut off / Heat Treatment	Through hole	Fork
As printed	M1#1	M1#2
Direct tempered 200°C	M2#1	M2#2
Direct tempered 650°C	M3#1	M3#2
Quenched & Tempered 200°C, 1h	M4#1	M4#2
Quenched & Tempered 650°C, 1h	M5#1	M5#2
Quenched & Tempered 200°C, 2h	M6#1	M6#2
Quenched & Tempered 650°C, 2h	M7#1	M7#2

E

Raw numbers, hardness test HV0.5, MX#1

Specimen	Depth [mm]	Hardness HV0.5
M1#1 Top	0,15	477
	0,2	413
	0,3	428
	0,4	451
	0,5	431
	1	429
	1,5	453
	2	418
	2,5	443
M1#1 OutsideMid	0,15	390
	0,2	398
	0,3	391
	0,4	391
	0,5	418
	1	424
	1,5	432
	2	421
	2,5	421
M1#1 InsideMid	0,15	414
	0,2	430
	0,3	421
	0,4	407
	0,5	413
	1	424
	1,5	421
	2	421
	2,5	424
M1#1 Bottom	0,15	357
	0,2	368
	0,3	370
	0,4	369
	0,5	402
	1	411
	1,5	420
	2	415
	2,5	417

Specimen	Depth [mm]	Hardness HV0.5
M2#1 Top	0,15	452
	0,2	404
	0,3	439
	0,4	418
	0,5	428
	1	436
	1,5	440
	2	440
	2,5	432
M2#1 OutsideMid	0,15	451
	0,2	392
	0,3	406
	0,4	409
	0,5	415
	1	430
	1,5	430
	2	414
	2,5	431
M2#1 InsideMid	0,15	432
	0,2	438
	0,3	424
	0,4	424
	0,5	423
	1	436
	1,5	421
	2	411
	2,5	422
M2#1 Bottom	0,15	365
	0,2	358
	0,3	372
	0,4	386
	0,5	406
	1	421
	1,5	414
	2	414
	2,5	440

Specimen	Depth [mm]	Hardness HV0.5
M3#1 Top	0,15	330
	0,2	320
	0,3	324
	0,4	319
	0,5	332
	1	329
	1,5	329
	2	332
	2,5	332
M3#1 OutsideMid	0,15	335
	0,2	332
	0,3	339
	0,4	335
	0,5	324
	1	315
	1,5	324
	2	316
	2,5	336
M3#1 InsideMid	0,15	327
	0,2	320
	0,3	342
	0,4	342
	0,5	313
	1	336
	1,5	322
	2	323
	2,5	325
M3#1 Bottom	0,15	318
	0,2	296
	0,3	319
	0,4	326
	0,5	309
	1	321
	1,5	314
	2	317
	2,5	331

Specimen	Depth [mm]	Hardness HV0.5
M4#1 Top	0,15	627
	0,2	612
	0,3	607
	0,4	596
	0,5	591
	1	596
	1,5	593
	2	599
	2,5	600
M4#1 OutsideMid	0,15	631
	0,2	612
	0,3	607
	0,4	552
	0,5	593
	1	571
	1,5	600
	2	584
	2,5	573
M4#1 InsideMid	0,15	609
	0,2	616
	0,3	582
	0,4	597
	0,5	559
	1	572
	1,5	586
	2	561
	2,5	559
M4#1 Bottom	0,15	630
	0,2	615
	0,3	600
	0,4	593
	0,5	578
	1	577
	1,5	583
	2	604
	2,5	571

Specimen	Depth [mm]	Hardness HV0.5
M5#1 Top	0,15	329
	0,2	311
	0,3	309
	0,4	303
	0,5	306
	1	299
	1,5	301
	2	304
	2,5	302
M5#1 OutsideMid	0,15	308
	0,2	309
	0,3	296
	0,4	307
	0,5	309
	1	309
	1,5	306
	2	303
	2,5	306
M5#1 InsideMid	0,15	316
	0,2	316
	0,3	313
	0,4	302
	0,5	307
	1	294
	1,5	307
	2	301
	2,5	312
M5#1 Bottom	0,15	317
	0,2	323
	0,3	311
	0,4	292
	0,5	305
	1	308
	1,5	308
	2	290
	2,5	305

Specimen	Depth [mm]	Hardness HV0.5
M6#1 Top	0,15	601
	0,2	594
	0,23	583
	0,4	587
	0,5	584
	1	580
	1,5	572
	2	577
	2,5	567
M6#1 OutsideMid	0,15	611
	0,2	587
	0,3	579
	0,4	579
	0,5	578
	1	582
	1,5	580
	2	586
	2,5	567
M6#1 InsideMid	0,15	613
	0,2	570
	0,3	577
	0,4	562
	0,5	573
	1,0	578
	1,5	586
	2,0	559
	2,5	561
M6#1 Bottom	0,15	603
	0,2	588
	0,3	572
	0,4	585
	0,5	537
	1,	554
	1,5	562
	2	545
	2,5	567

Specimen	Depth [mm]	Hardness HV0.5
M7#1 Top	0,15	325
	0,2	320
	0,3	310
	0,4	305
	0,5	298
	1	304
	1,5	298
	2	309
	2,5	305
M7#1 OutsideMid	0,15	328
	0,2	305
	0,3	298
	0,4	310
	0,5	295
	1	308
	1,5	311
	2	308
	2,5	310
M7#1 InsideMid	0,15	310
	0,2	315
	0,3	305
	0,4	295
	0,5	302
	1	304
	1,5	307
	2	298
	2,5	306
M7#1 Bottom	0,15	325
	0,2	305
	0,3	305
	0,4	305
	0,5	299
	1	299
	1,5	303
	2	304
	2,5	306

F

Hardness test HV0.5, MX#2

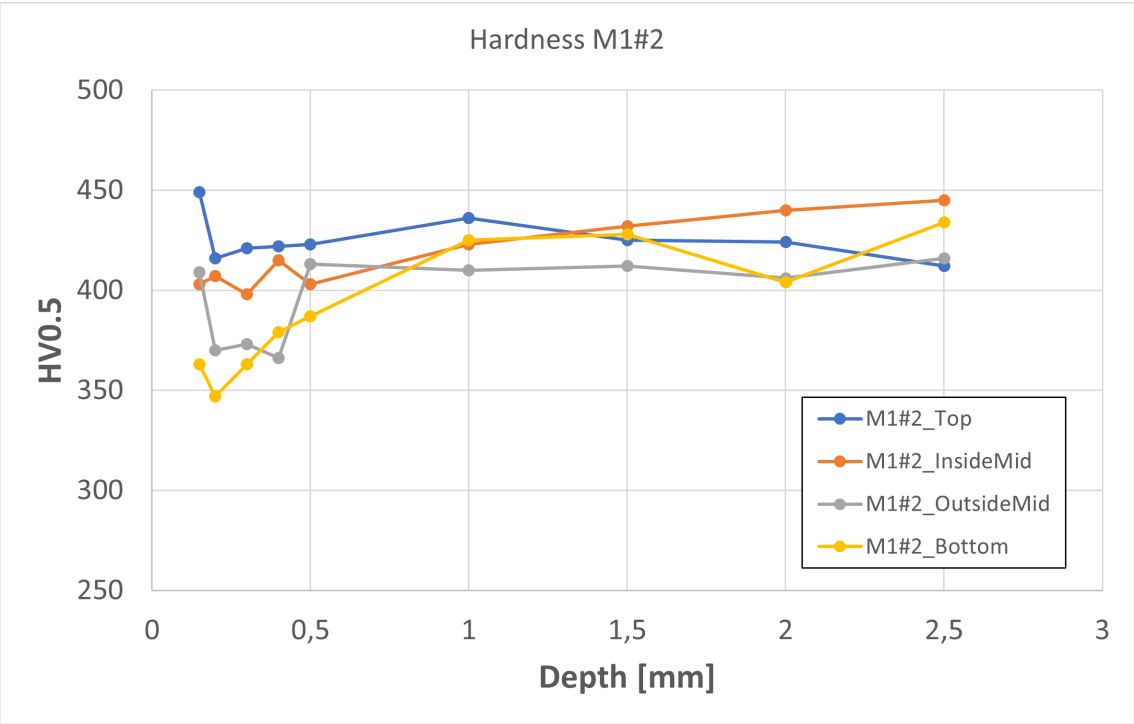

Figure F.1: Hardness profile for Sample M1#2, the fork of the yoke

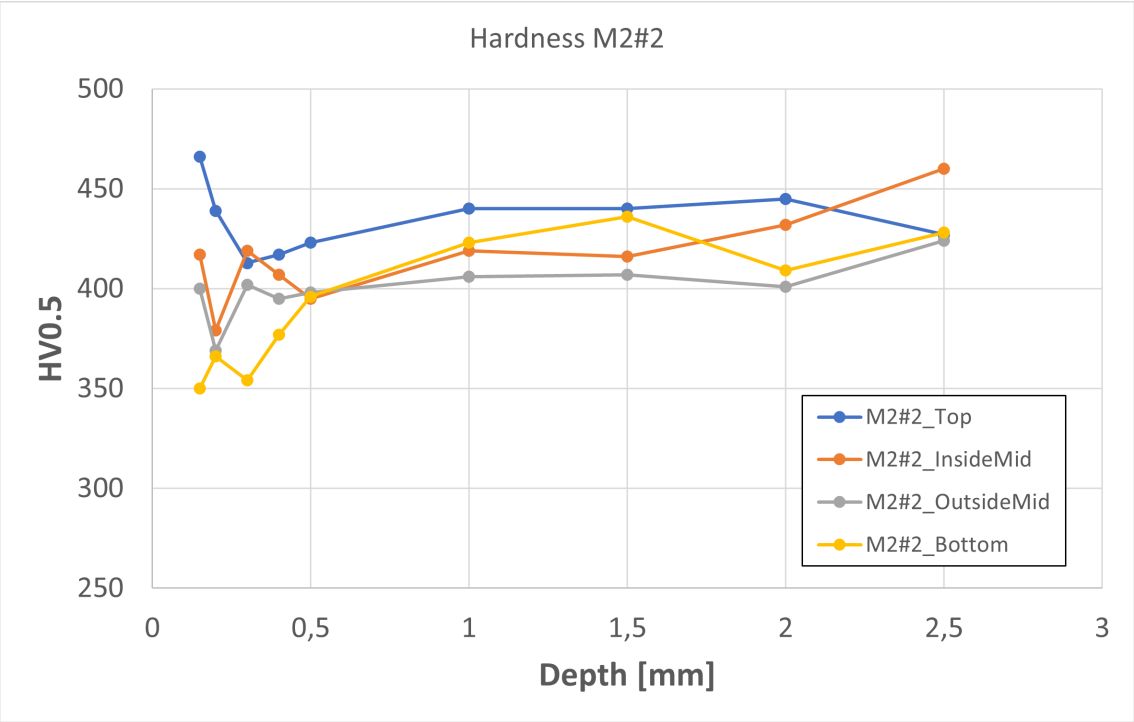

Figure F.2: Hardness profile for Sample M2#2, the fork of the yoke

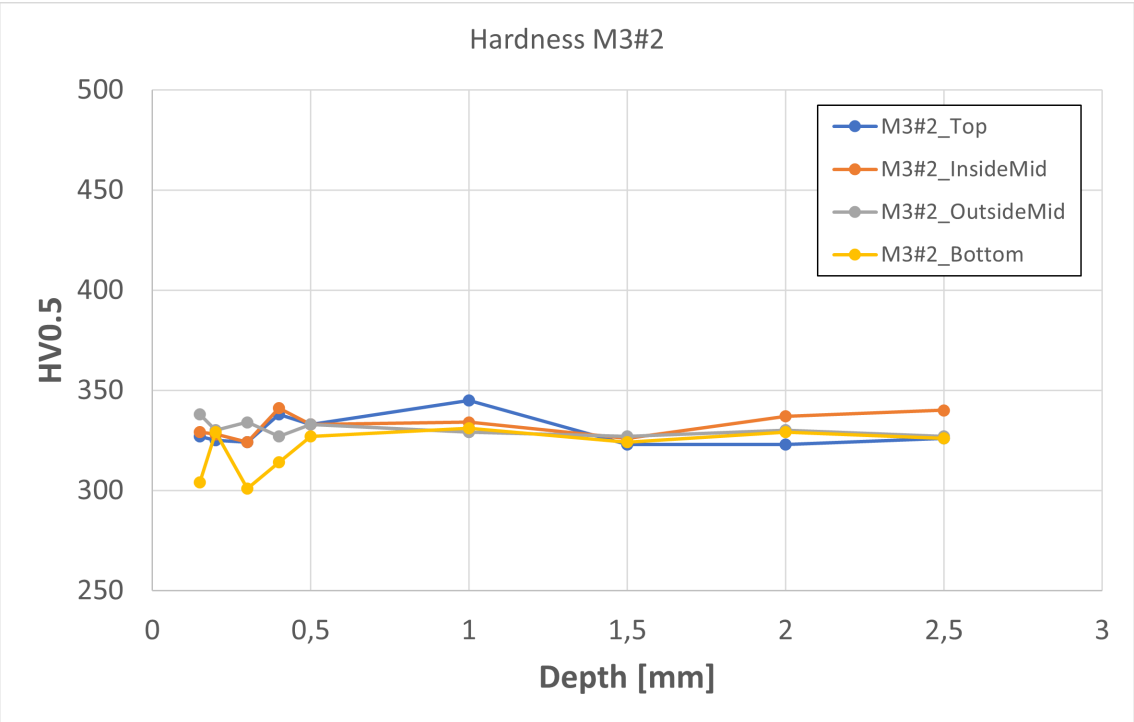

Figure F.3: Hardness profile for Sample M3#2, the fork of the yoke

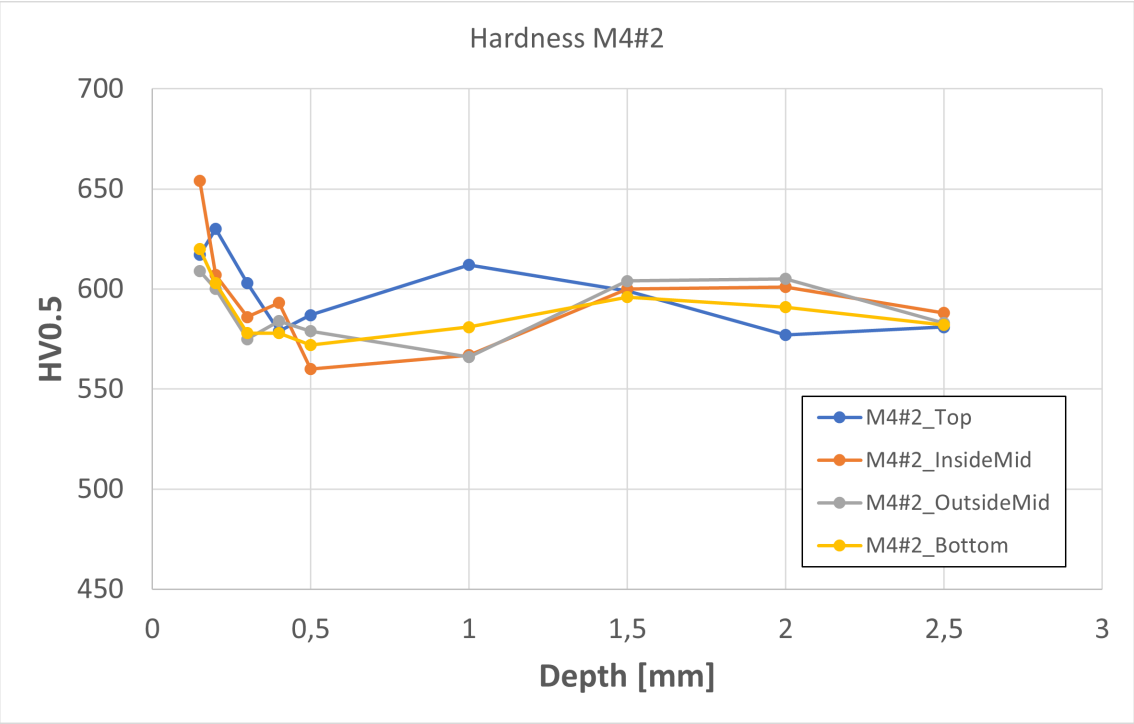

Figure F.4: Hardness profile for Sample M4#2, the fork of the yoke

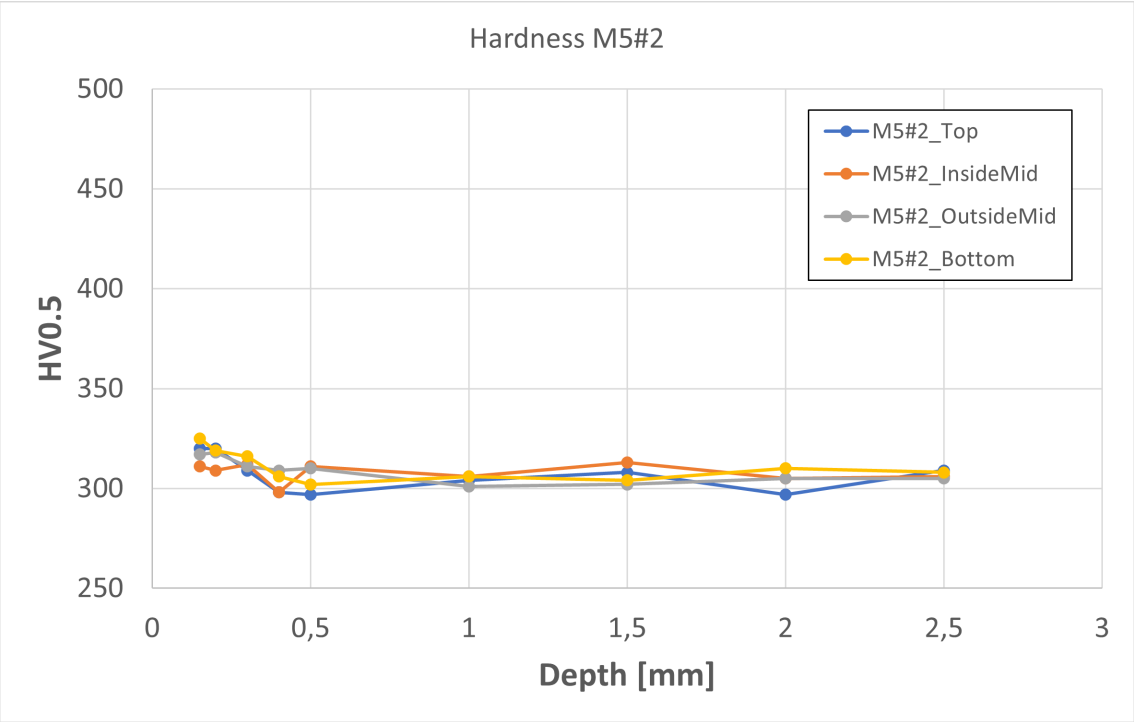

Figure F.5: Hardness profile for Sample M5#2, the fork of the yoke

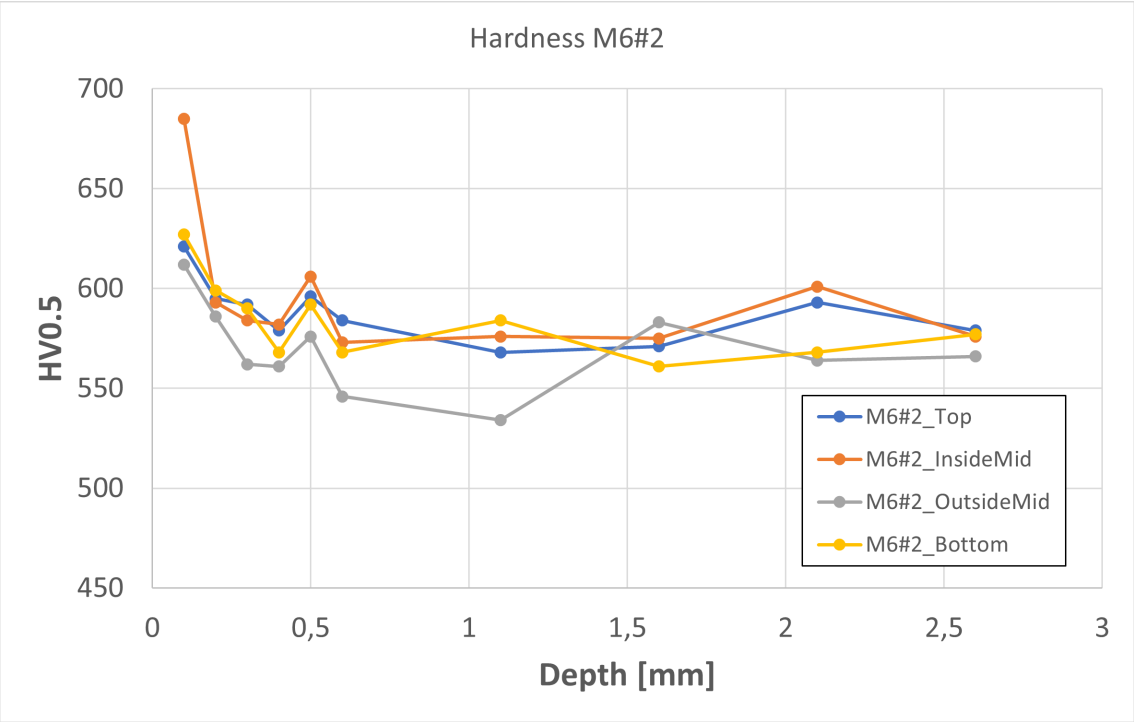

Figure F.6: Hardness profile for Sample M6#2, the fork of the yoke

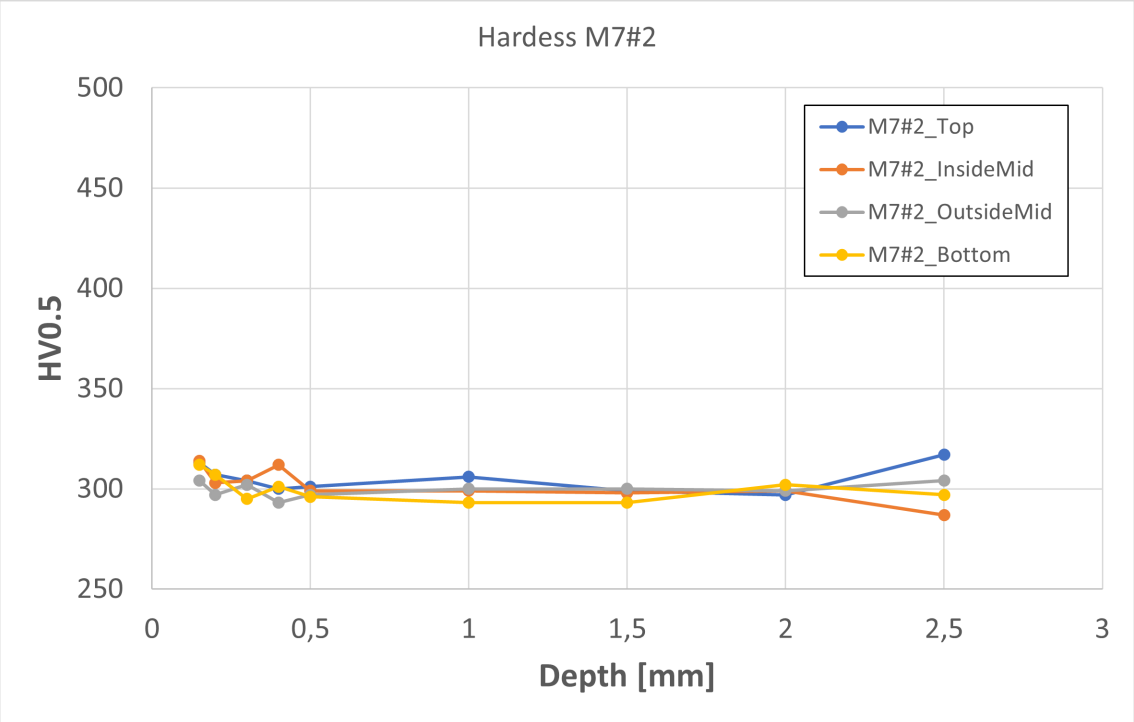

Figure F.7: Hardness profile for Sample M7#2, the fork of the yoke

F.1 Raw numbers MX#2

Specimen	Depth [mm]	Hardness HV0.5
M1#2 Top	0,15	449
	0,2	416
	0,3	421
	0,4	422
	0,5	423
	1	436
	1,5	425
	2	424
	2,5	412
M1#2 InsideMid	0,15	403
	0,2	407
	0,3	398
	0,4	415
	0,5	403
	1	423
	1,5	432
	2	440
	2,5	445
M1#2 OutsideMid	0,15	409
	0,2	370
	0,3	373
	0,4	366
	0,5	413
	1	410
	1,5	412
	2	406
	2,5	416
M1#2 Bottom	0,15	363
	0,2	347
	0,3	363
	0,4	379
	0,5	387
	1	425
	1,5	428
	2	404
	2,5	434

Specimen	Depth [mm]	Hardness HV0.5
M2#2 Top	0,15	466
	0,2	439
	0,3	413
	0,4	417
	0,5	423
	1	440
	1,5	440
	2	445
	2,5	427
M2#2 InsideMid	0,15	417
	0,2	379
	0,3	419
	0,4	407
	0,5	395
	1	419
	1,5	416
	2	432
	2,5	460
M2#2 OutsideMid	0,15	400
	0,2	369
	0,3	402
	0,4	395
	0,5	398
	1	406
	1,5	407
	2	401
	2,5	424
M2#2 Bottom	0,15	350
	0,2	366
	0,3	354
	0,4	377
	0,5	396
	1	423
	1,5	436
	2	409
	2,5	428

Specimen	Depth [mm]	Hardness HV0.5
M3#2 Top	0,15	327
	0,2	325
	0,3	324
	0,4	338
	0,5	333
	1	345
	1,5	323
	2	323
	2,5	326
M3#2 InsideMid	0,15	329
	0,2	328
	0,3	324
	0,4	341
	0,5	333
	1	334
	1,5	326
	2	337
	2,5	340
M3#2 OutsideMid	0,15	338
	0,2	330
	0,3	334
	0,4	327
	0,5	333
	1	329
	1,5	327
	2	330
	2,5	327
M3#2 Bottom	0,15	304
	0,2	329
	0,3	301
	0,4	314
	0,5	327
	1	331
	1,5	324
	2	329
	2,5	326

Specimen	Depth [mm]	Hardness HV0.5
M4#2 Top	0,1	617
	0,2	630
	0,3	603
	0,4	579
	0,5	587
	1,0	612
	1,5	599
	2	577
	2,5	581
M4#2 InsideMid	0,15	654
	0,2	607
	0,3	586
	0,4	593
	0,5	560
	1	567
	1,5	600
	2	601
	2,5	588
M4#2 OutsideMid	0,15	609
	0,2	600
	0,3	575
	0,4	584
	0,5	579
	1	566
	1,5	604
	2,0	605
	2,5	583
M4#2 Bottom	0,15	620
	0,2	603
	0,3	578
	0,4	578
	0,5	572
	1	581
	1,5	596
	2	591
	2,5	582

Specimen	Depth [mm]	Hardness HV0.5
M5#2 Top	0,15	320
	0,2	320
	0,3	309
	0,4	298
	0,5	297
	1	304
	1,5	308
	2	297
	2,5	309
M5#2 InsideMid	0,15	311
	0,2	309
	0,3	312
	0,4	298
	0,5	311
	1	306
	1,5	313
	2	305
	2,5	306
M5#2 OutsideMid	0,15	317
	0,2	318
	0,3	311
	0,4	309
	0,5	310
	1	301
	1,5	302
	2	305
	2,5	305
M5#2 Bottom	0,15	325
	0,2	319
	0,3	316
	0,4	306
	0,5	302
	1	306
	1,5	304
	2	310
	2,5	308

Specimen	Depth [mm]	Hardness HV0.5
M6#2 Top	0,1	621
	0,2	595
	0,3	592
	0,4	579
	0,5	596
	0,6	584
	1,1	568
	1,6	571
	2,1	593
	2,6	579
M6#2 InsideMid	0,1	685
	0,2	593
	0,3	584
	0,4	582
	0,5	606
	0,6	573
	1,1	576
	1,6	575
	2,1	601
	2,6	576
M6#2 OutsideMid	0,1	612
	0,2	586
	0,3	562
	0,4	561
	0,5	576
	0,6	546
	1,1	534
	1,6	583
	2,1	564
	2,6	566
M6#2 Bottom	0,1	627
	0,2	599
	0,3	590
	0,4	568
	0,5	592
	0,6	568
	1,1	584
	1,6	561
	2,1	568
	2,6	577

Specimen	Depth [mm]	Hardness HV0.5
M7#2 Top	0,15	313
	0,2	307
	0,3	304
	0,4	300
	0,5	301
	1	306
	1,5	299
	2	297
	2,5	317
M7#2 InsideMid	0,15	314
	0,2	303
	0,3	304
	0,4	312
	0,5	299
	1	299
	1,5	298
	2	299
	2,5	287
M7#2 OutsideMid	0,15	304
	0,2	297
	0,3	302
	0,4	293
	0,5	297
	1	300
	1,5	300
	2	299
	2,5	304
M7#2 Bottom	0,15	312
	0,2	307
	0,3	295
	0,4	301
	0,5	296
	1	293
	1,5	293
	2	302
	2,5	297

G

Raw numbers, hardness test HK, MX#1

Specimen	Depth [mm]	Hardness HK0.2
M1#1	0,025	644
	0,04	669
	0,05	691
	0,065	732
	0,15	523
	0,2	502
	0,5	488
	1	552
M2#1	0,025	631
	0,04	664
	0,05	683
	0,065	675
	0,15	525
	0,2	497
	0,5	562
	1	519
M3#1	0,025	358
	0,04	354
	0,05	378
	0,065	400
	0,15	372
	0,2	386
	0,5	362
	1	380
M4#1	0,025	747
	0,04	763
	0,05	800
	0,065	732
	0,15	688
	0,2	675
	0,5	651
	1	646

Specimen	Depth [mm]	Hardness HK0.2
M5#1	0,025	357
	0,04	385
	0,05	373
	0,065	374
	0,15	357
	0,2	344
	0,5	333
	1	352
M6#1	0,025	711
	0,04	700
	0,05	751
	0,065	688
	0,15	697
	0,2	723
	0,5	669
	1	641
M7#1	0,03	355
	0,04	354
	0,06	358
	0,07	368
	0,15	327
	0,2	347
	0,5	325
	1	338

DEPARTMENT OF INDUSTRIAL AND MATERIALS SCIENCE
CHALMERS UNIVERSITY OF TECHNOLOGY
Gothenburg, Sweden
www.chalmers.se

CHALMERS
UNIVERSITY OF TECHNOLOGY